Natural and drought scenarios in an east central Amazon forest: Fidelity of the Community Land Model 3.5 with three biogeochemical models

Koichi Sakaguchi,[1] Xubin Zeng,[1] Bradley J. Christoffersen,[2] Natalia Restrepo-Coupe,[2] Scott R. Saleska,[2] and Paulo M. Brando[3]

Received 8 July 2010; revised 9 November 2010; accepted 23 November 2010; published 12 March 2011.

[1] Recent development of general circulation models involves biogeochemical cycles: flows of carbon and other chemical species that circulate through the Earth system. Such models are valuable tools for future projections of climate, but still bear large uncertainties in the model simulations. One of the regions with especially high uncertainty is the Amazon forest where large-scale dieback associated with the changing climate is predicted by several models. In order to better understand the capability and weakness of global-scale land-biogeochemical models in simulating a tropical ecosystem under the present day as well as significantly drier climates, we analyzed the off-line simulations for an east central Amazon forest by the Community Land Model version 3.5 of the National Center for Atmospheric Research and its three independent biogeochemical submodels (CASA', CN, and DGVM). Intense field measurements carried out under Large Scale Biosphere-Atmosphere Experiment in Amazonia, including forest response to drought from a throughfall exclusion experiment, are utilized to evaluate the whole spectrum of biogeophysical and biogeochemical aspects of the models. Our analysis shows reasonable correspondence in momentum and energy turbulent fluxes, but it highlights three processes that are not in agreement with observations: (1) inconsistent seasonality in carbon fluxes, (2) biased biomass size and allocation, and (3) overestimation of vegetation stress to short-term drought but underestimation of biomass loss from long-term drought. Without resolving these issues the modeled feedbacks from the biosphere in future climate projections would be questionable. We suggest possible directions for model improvements and also emphasize the necessity of more studies using a variety of in situ data for both driving and evaluating land-biogeochemical models.

Citation: Sakaguchi, K., X. Zeng, B. J. Christoffersen, N. Restrepo-Coupe, S. R. Saleska, and P. M. Brando (2011), Natural and drought scenarios in an east central Amazon forest: Fidelity of the Community Land Model 3.5 with three biogeochemical models, *J. Geophys. Res.*, *116*, G01029, doi:10.1029/2010JG001477.

1. Introduction

[2] Facing the impact of the climate change on human societies and ecosystems, much attention is being paid to future climate projections. A critical, yet poorly understood constraint on such projections is the effect that the biosphere exerts back on the climate system [*Meehl et al.*, 2007]. Over the continents, changes in climate will alter the distribution and composition of vegetation cover, which not only affect biophysical factors such as surface momentum exchange and energy balance, but the cycling of carbon and other trace gases in the atmosphere as well. The latter, or so-called biogeochemical cycles (BGC), until recently have not been part of future climate projections. Coupled BGC–general circulation models, while still in infancy, represent our best understanding of such atmosphere-land interactions [e.g., *Friedlingstein et al.*, 2006; *Thornton et al.*, 2009], and predict that even regional alterations in BGC exhibit a significant effect on the global climate system and demonstrate the possibility of positive feedback loops. Coupled BGC models are expected to play a more important role than before, for example, in the next assessment report by the Intergovernmental Panel on Climate Change [*Taylor et al.*, 2009]. However, recent intercomparison studies of BGC models show that there is a large disparity on the modeled response of ecosystems to the increasing CO_2 and associated change in the climate system [*Friedlingstein et al.*, 2006; *Sitch et al.*, 2008].

[3] A region with particularly high uncertainty is the Amazon rain forest, the world's largest contiguous forest

[1]Department of Atmospheric Sciences, University of Arizona, Tucson, Arizona, USA.
[2]Department of Ecology and Evolutionary Biology, University of Arizona, Tucson, Arizona, USA.
[3]Instituto de Pesquisa Ambiental da Amazônia, Brasilia, Brazil.

0148-0227/11/2010JG001477

that stores about 10–15% of total global above ground biomass [*Potter*, 1999; *Houghton et al.*, 2001; *Malhi et al.*, 2006] and changes in vegetation cover can affect the regional and global climate [*Eltahir and Bras*, 1994; *Malhi et al.*, 2008; *Betts and Silva Dias*, 2010]. Observations and modeling indicate that this region has higher probability of drought intensification [*Malhi et al.*, 2008] and is among the more vulnerable to future climate-induced savannization [*Hutyra et al.*, 2005]. A large part of the uncertainty for the predicted future of the Amazon forest can be attributed to the representation of the vulnerability of the forest to large-scale dieback in a class of BGC models called Dynamic Global Vegetation Models (DGVMs,) which are developed to simulate spatiotemporal relative abundances of Plant Functional Types (PFTs) in response to climate conditions [*Oyama and Nobre*, 2003; *Cox et al.*, 2004; *Bonan and Levis*, 2006; *Salazar et al.*, 2007; *Sitch et al.*, 2008; *Huntingford et al.*, 2008; *Malhi et al.*, 2009a]. These modeling studies implicate various causes of dieback, some emphasizing the direct effects of the increased air temperatures on plant physiology [*Galbraith et al.*, 2010], while others emphasize a strong role of stomatal conductance: rising CO_2 and initial decreases in precipitation and/or increase in evaporative demand prompt stomatal closure and reduction in transpiration [*Betts et al.*, 2004].

[4] The realism of the dieback and its possible causes simulated in these models are, however, not necessarily robust. For example, *Saleska et al.* [2003] showed that previous generations of land surface and ecological models were not able to reproduce the vegetation productivity during dry seasons, presumably supported by deep root systems, in an east central Amazon site. The effect of the increased CO_2 concentration and other environmental drivers on photosynthesis [*Lloyd and Farquhar*, 2008; *Doughty and Goulden*, 2008b] and respiration [*Wright et al.*, 2006; *Meir et al.*, 2008], as well as the mortality mechanism from drought stress [*McDowell et al.*, 2008] are still active subjects of field-based studies and a part of the uncertainties in BGC modeling. Furthermore, most of the aforementioned DGVMs are subject to computational constraints associated with capturing dynamic global plant biogeography, thus the usual PFT approach in which several (5–20) PFTs differ in selected ecophysiological traits necessitates much simplification of vegetation dynamics [*Smith et al.*, 2001; *Purves and Pacala*, 2008]. In the case of the Amazon forest, further complicating the picture is that recent observations during a short but vast and intense drought in the Amazon basin in 2005 revealed a near-instantaneous large-scale vegetation greening in the short term [*Saleska et al.*, 2007] (but see *Samanta et al.* [2010]), but also increased tree mortality resulting in large losses of carbon when integrated over multiple years [*Phillips et al.*, 2009].

[5] On the other hand, the increasing availability and understanding in eddy flux measurements [*Wilson et al.*, 2002; *Baldocchi*, 2003; *da Rocha et al.*, 2009] and its combined use with biometric observations [*Saleska et al.*, 2003] can provide strong constraints to model developments. In order to better evaluate and develop land-BGC models, it is necessary to exploit the full potential that the combination of in situ meteorological, flux, and biometric measurements have to respectively drive and evaluate them, which is only now being realized [e.g., *Kucharik et al.*, 2006; *Desai et al.*, 2007; L. G. de Goncalves et al., The Large Scale Biosphere-Atmosphere Experiment in Amazônia, Model Intercomparison Project (LBA-MIP) protocol, version 3.0, obtained from http://www.climatemodeling.org/lba-mip/on 20 June 2008]. Such a rigorous and integrated assessment is critical for the study of carbon cycle models because unlike the surface energy budget, the carbon budget is not necessarily balanced at the land surface but instead it requires knowledge of behavior of storage pools. In other words, small errors from unreasonable assumptions, incorrect extrapolation from small to large-scale processes (e.g., leaf to canopy), or inconsistent input data can accumulate over time and change equilibrium states. If, for example, the scaling of leaf to canopy for flux exchanges are tuned to erroneous biomass structures, then the critical link between the biosphere and climate could not be simulated reliably for the future. Furthermore, most model evaluation has been carried out under normal climate scenarios. A relatively unexplored avenue for BGC models and DGVMs in particular, is to utilize in situ forcing data to mirror large-scale experimental manipulation and validate the models with rich data sets available assessing vegetation response to disturbances. Artificial drought experiments conducted in the eastern Amazon forest can provide such opportunities [*Nepstad et al.*, 2007; *da Costa et al.*, 2010].

[6] With the wide variety of in situ data sets, we aim to address a key question for the future projection of the Amazon Forest: Is the current generation of global land/BGC models able to reliably simulate the response of the Amazon ecosystem to changing climate, including drought mortality? If not, then we need to clarify what improvements are necessary. We approach this question by one of the widely used global land models, the National Center for Atmospheric Research (NCAR) Community Land Model 3.5 (CLM3.5) [*Oleson et al.*, 2008], coupled independently to three BGC submodels (CASA', CN, and DGVM, explained in section 2) with in situ input data and at a corresponding single point scale. CLM3.5 is a test bed model for various new and unique parameterizations that include explicit aquifer models and improved canopy integration for photosynthesis, among many others. Newly added parameterizations are designed primarily to remove the dry bias in soil moisture in the previous version, which was not able to realistically simulate the atmosphere-land interactions in the Amazon forest [*Bonan and Levis*, 2006; *Dickinson et al.*, 2006]. Several studies showed better model performance with these new parameterizations in energy and water cycles [*Lawrence et al.*, 2007; *Stöckli et al.*, 2008a; *Oleson et al.*, 2008]. The carbon cycle simulated by CLM3.5 and two of the BGC models (CASA' and CN) were studied by *Randerson et al.* [2009] and found to grossly overestimate the live above ground biomass (LAGB) in the Amazon. However, their analysis may have suffered in part from input data biases coming from the use of global-scale data, or the scale difference between the model grid and point measurements.

[7] We first evaluate the model performance under present climate with the focuses on (1) the simulated flux exchanges (momentum, energy, water, and carbon) at daily-seasonal timescales, and (2) the simulated vegetation structure (carbon

Table 1. List of Symbols and Acronyms Used in the Main Text

Symbol/Acronym	Description
ANPP	Aboveground net primary production (MgC ha^{-1} yr^{-1})
BGC	Biogeochemical cycles
CASA'	One of the three CLM3.5 BGC submodels
CLM	Community Land Model
CN	One of the three CLM3.5 BGC submodels
CWD	Coarse woody debris
dbh	Diameter at breast height (cm)
DGVM	Dynamic Global Vegetation Model, also one of the three CLM3.5 BGC submodels
GPP	Gross primary productivity ($\mu molCO_2$ m^{-2} s^{-1})
H	Sensible heat flux (W m^{-2})
LAGB	Live aboveground biomass (MgC ha^{-1})
LAI	Leaf area index
LBA	Large-Scale Biosphere-Atmosphere Experiment in Amazonia
LE	Latent heat flux (W m^{-2})
LUE	Light use efficiency, the initial slope of GPP–photosynthetically active radiation relationship
MBE	Mean Bias Error
NCAR	National Center for Atmospheric Research
NEE	Net ecosystem exchange ($\mu molCO_2$ m^{-2} s^{-1})
NoBGC	The experiment in which CLM3.5 is not coupled to any BGC models
PFT	Plant Functional Type
r	Correlation coefficient
Ra	Autotrophic respiration ($\mu molCO_2$ m^{-2} s^{-1})
Reco	Ecosystem respiration ($\mu molCO_2$ m^{-2} s^{-1}), Reco = Ra + Rh
Rh	Heterotrophic respiration ($\mu molCO_2$ m^{-2} s^{-1})
RMSE	Root Mean Square Error
σ_n	Normalized standard deviation, simulated standard deviation divided by the observed standard deviation
SLA	Specific Leaf Area (m^2 gC^{-1})
SOC	Soil organic carbon (MgC ha^{-1})
TEE	Throughfall Exclusion Experiment
τ	Momentum flux (kg m^{-1} s^{-2})
TWC	Total water content (mm) in the top 2 m of the soil column
VWC	Volumetric water content (m^3 m^{-3})

pool size) and its link to biogeophysical processes. Then we assess the capability of these models in projecting die-off events under drier climate by simulating an artificial drought field experiment and comparing the observed and modeled ecosystem responses. Success or failure of the new parameterizations in CLM3.5 would help further developments of CLM and other land/BGC models. Our unique model evaluation under drought conditions provides a quantitative measure of global-scale BGC model skills under transient climate. The evaluations are based on the observations in an east central Amazonian forest under the Large-Scale Biosphere-Atmosphere Experiment in Amazonia (LBA) [*Keller et al.*, 2004]. Several symbols and acronyms used in the text are summarized in Table 1.

2. Methods

2.1. Site and Data Description

2.1.1. KM67 Site and Eddy Covariance Measurements

[8] LBA project has established a network of eddy covariance towers across a range of biome types and climate regimes in the Amazon basin, known as Brasilflux [*da Rocha et al.*, 2009]. The tower used in this study is KM67, located in the Tapajós National Forest (2.86°S, 54.96°W) (Figure 1a). The forest receives ~2000 mm of annual rainfall on average and experiences ~5 months long dry season with monthly rainfall < 100 mm (Figure 1b). The site is surrounded by an evergreen moist tropical forest that maintains a high leaf area index (LAI) throughout the year. The tower is situated atop of a flat plateau consisting of a highly weathered and deep clay-rich oxisol with smaller coverage of sandy ultisols [*Silver et al.*, 2000]. Further site characteristics are described by *Rice et al.* [2004] and *Hutyra et al.* [2007].

[9] The flux data of momentum (τ), sensible heat (H), latent heat (LE), and net ecosystem exchange (NEE) of CO_2 are obtained for the years 2002–2004. The reader is referred to *Saleska et al.* [2003] and *Hutyra et al.* [2007] and their supplements for details of instrumentation, flux calculations and quality control procedures, which are only summarized here. Flux measurements were made above the canopy at 57.8 m height, and at eight different heights temperature as well as CO_2 concentration were measured to estimate the storage of heat and CO_2 in the canopy air. NEE is defined as the sum of the CO_2 flux at the top of the tower and the change in canopy CO_2 storage, and it is corrected for low turbulent conditions (friction velocity < 0.22 m s^{-1}) in order to estimate the biological contribution to NEE, independent of the atmospheric stability as much as possible. Ecosystem respiration (Reco) was calculated from the nighttime measurement of NEE, assuming it is independent of air temperature; gross primary productivity (GPP) was obtained as the difference between NEE and Reco. Instrumental failures and other unfavorable conditions (e.g., precipitation) also caused 15~25% of the data to be missing, which were filled by similar methods to those employed during low turbulence periods. In all our evaluation exercises we avoid nighttime or daytime bias by only using the days with full 24 hourly measurements. When there are less than 30% of daily means available for a given month, we did not use that month for obtaining a monthly mean. The annual energy balance closure is, on average, 85% when the canopy air heat content is considered; incomplete closure is typical with eddy covariance studies, but not necessarily represents the bias in the turbulent flux measurements since some of the imbalance can be attributed, for example, to the scale and target differences among the eddy flux and other energy measurements [*Wilson et al.*, 2002; *Baldocchi*, 2003].

[10] Ground-based measurements on vegetation and soil carbon stocks have been reported in several studies at the Tapajós National Forest [e.g., *Silver et al.*, 2000; *Rice et al.*, 2004; *Pyle et al.*, 2008; *Quesada et al.*, 2009], which provide valuable information to evaluate the simulated carbon

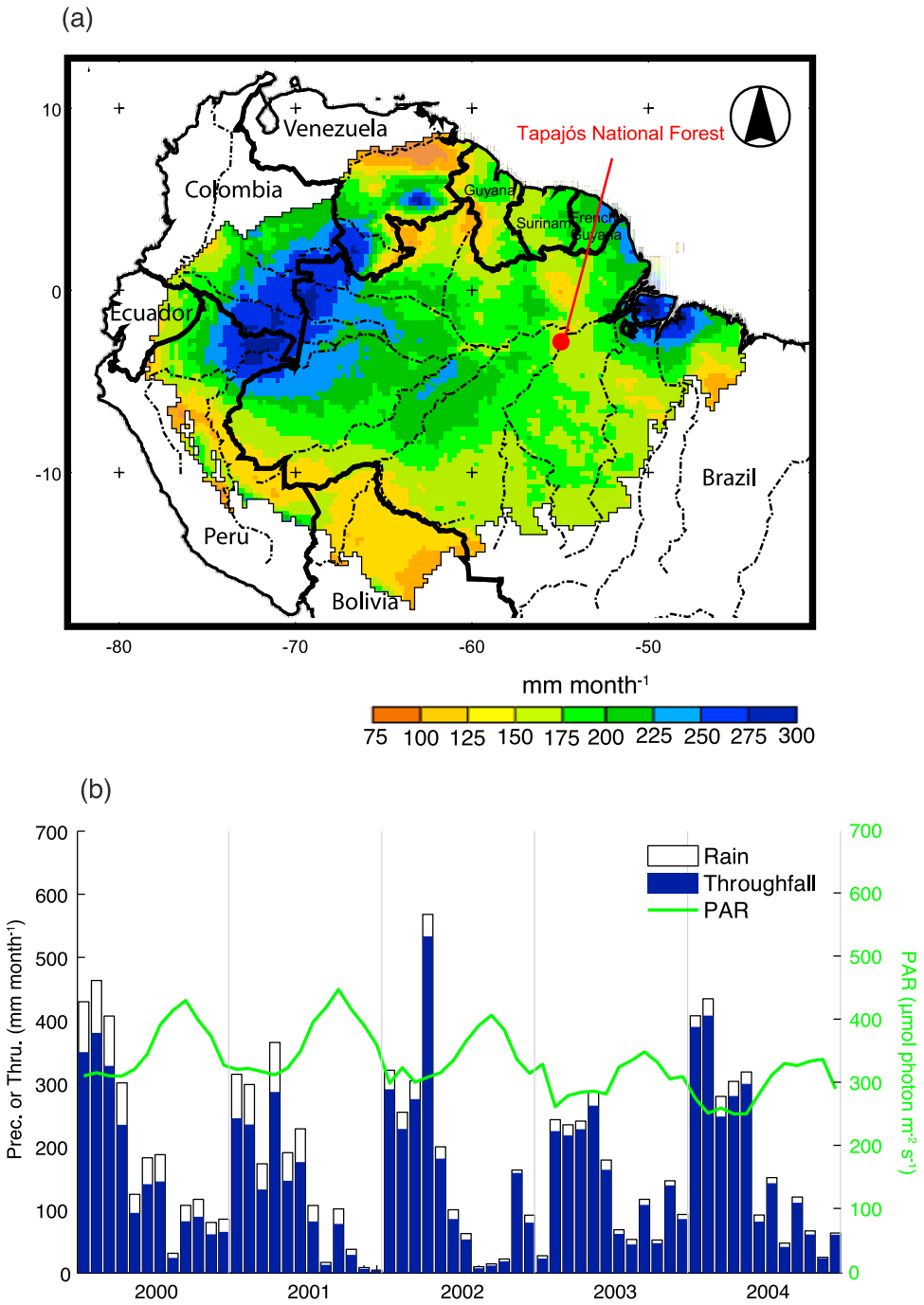

Figure 1. Study site characteristics. (a) Location of the study site, Tapajós National Forest (red dot) and climatological (1998–2006) monthly precipitation from Tropical Rainfall Measuring Mission (color shading) [*NASA*, 2007], and (b) time series of the monthly precipitation and simulated throughfall for the natural (nondrought condition) condition, superimposed by monthly mean photosynthetically active radiation (PAR).

pool sizes. Those biometric measurements were synthesized by *Malhi et al.* [2009b], and our model-to-observation comparison is mostly made based on their synthesis.

2.1.2. Throughfall Exclusion Experiment

[11] In 1999, a 5 year Throughfall Exclusion Experiment (TEE) was initiated ~4.5 km south of the KM67 tower to assess, in situ, the forest response to artificial drought. Drought effects on the evergreen tropical forest were studied by comparing a 1 ha control plot with a nearby 1 ha treatment plot where a portion of throughfall was excluded by clear plastic panels and wooden gutters during the wet season (January–July) from 2000 to 2004. The plastic panels and wooden gutters caused only a small increase of the forest floor temperature by ~0.3°C. Each plot was partially isolated from the surrounding forest by soil trenches of ≥1 m depth to minimize the lateral movement of water and roots.

Table 2. Summary of the Three Biogeochemical Submodels for CLM3.5[a]

Model Name	CASA'	CN	DGVM
Base model	CASA [*Potter et al.*, 1993; *Friedlingstein et al.*, 1999]	BIOME-BGC [*Thornton et al.*, 2002; *Thornton and Rosenbloom*, 2005]	LPJ and IBIS [*Foley et al.*, 1996; *Sitch et al.*, 2003]
C cycle	yes	yes	yes
N cycle	no	yes	no
Plant dynamics (change in PFT cover)	no	no	yes
Number of C pools	3 plant tissues, 5 litter pools, 2 microbial communities, 2 SOC	6 plant tissues, 14 plant internal pools, 4 litter pools, 4 SOC.	4 plant tissues, 2 litter pools, 2 SOC
R_a	50% of GPP	R_m: Depends on N and T (Q_{10}) R_g: 30% of new growth carbon	R_m: Depends on C and T [*Lloyd and Taylor*, 1994] R_g: 25% of (GPP-R_m)
R_h	Depends on C, θ, T (Q_{10})	Depends on C, N, Ψ, and T [*Lloyd and Taylor*, 1994]	Depends on C, θ, and T [*Lloyd and Taylor*, 1994]
Carbon allocation among plant tissue types	Updated every time step, maximize resource acquisition assumption	Updated every time step, maximize resource acquisition within allometric constraints	Updated yearly, maximize resource acquisition within allometric constraints
Vertical distribution of root fraction	Exponential decrease (from base model CLM3.5)	Linear decrease	Exponential decrease (from base model CLM3.5)
Leaf phenology	Single phenology scheme with growing degree days summation, Based on *Dickinson et al.* [1998]	Four types: evergreen, seasonal-deciduous, warm stress-deciduous, cold stress-deciduous. Based on *White et al.* [1997]	Four types: evergreen, seasonal-deciduous, stress-deciduous, grass. Based on IBIS and LPJ models

[a]SOC, soil organic carbon; C, carbon; N, nitrogen; T, temperature; θ, volumetric soil water content; Ψ, soil water potential; R_a, autotrophic respiration; R_h, heterotrophic respiration; R_m, plant maintenance respiration; R_g, plant growth respiration, with $R_a = R_m + R_g$.

The effect of the exclusion treatment was analyzed by comparing a wide range of physical and biological measurements from the two plots, including, but not limited to, biomass, LAI [*Nepstad and Mountinho*, 2008b], Specific Leaf Area (SLA, $m^2\ gC^{-1}$) [*Nepstad and Mountinho*, 2009a], litterfall [*Nepstad and Mountinho*, 2010], stem mortality, aboveground net primary production (ANPP), and soil water content [*Nepstad and Mountinho*, 2009b]. Through the 5 year drought experiment, they found significant differences in the aboveground wood production and mortality between the control and TEE plots, although it took about 2 years for the effect of drought to become substantial. The reader is referred to *Nepstad et al.* [2002] for further details on site characteristics, experimental design, and measurements.

2.2. Model Descriptions: Biogeophysics and Biogeochemistry

[12] The NCAR CLM simulates a suite of near-surface processes, including radiative transfer, snow and soil physics, and turbulent exchange at subhourly time steps. A model grid is represented as a combination of subgrid land cover types of glacier, lake, wetland, urban, and vegetated land. Within the vegetated land fraction, a PFT approach is used [see *Bonan et al.*, 2003] to classify vegetation based on climate zones, height, photosynthetic parameters, and rooting distribution; PFT relative abundances must be specified for nondynamic vegetation simulations. Also specified for non-BGC simulations is LAI and canopy height.

[13] CLM3.5 is the transitional model from the earlier version 3.0 with significant modifications to its soil hydrology and other biogeophysical components [*Oleson et al.*, 2004, 2008]. One of the major changes is the soil bottom boundary condition from "free drainage" in CLM3.0 to interactive groundwater schemes [*Niu et al.*, 2007]. Another improvement in the model's realism is the computation of leaf-level photosynthesis and its scaling to the canopy level. Leaf-level photosynthesis is calculated following *Farquhar et al.* [1980] and *Collatz et al.* [1991] with the distinction of the sunlit and shaded fraction of leaves, as well as direct and diffuse radiation [*Dai et al.*, 2004]. It also considers the difference in SLA over sunlit and shaded leaves as well as across the vertical canopy gradient [*Thornton and Zimmermann*, 2007] to integrate photosynthesis from individual leaf to canopy level. Autotrophic and heterotrophic respiration (Ra, Rh, respectively) and terrestrial carbon pools are not by default simulated in CLM3.5; one of the three available BGC submodels are necessary to be run together for full carbon cycle simulations. The three BGC models share some formulations and model structures (e.g., all of them use the photosynthesis model in CLM3.5), but also differ in several aspects reflecting different assumptions and main target processes to simulate (see Table 2). Some of the most relevant equations in these models are provided in Appendices A and B, while further details are provided in the relevant references cited. We should note that the improved photosynthesis model in CLM3.5 by *Thornton and Zimmermann* [2007] was designed mainly for CLM3.5-CN combination, thus the performance in carbon balance could be lower when either CASA' or DGVM are coupled.

[14] CASA' is a modified version of the terrestrial biogeochemical model CASA, which was originally developed to model seasonal and interannual variability of carbon and nitrogen dynamics in the atmosphere-plant-soil systems at a global scale [*Potter et al.*, 1993; *Friedlingstein et al.*, 1999]. Its developmental changes and the results from the simulations coupled to NCAR general circulation models are reported by *Fung et al.* [2004] and *Doney et al.* [2006]. CASA' inherits the representation of carbon pools in vegetation, litter, and soil from the original model, but it excludes the prognostic nitrogen cycle. The litter pools are partitioned

into surface, soil, and coarse woody debris pools that receive carbon from dead leaves, roots, and woody tissues, respectively. The surface and soil litter pools are further partitioned into metabolic and structure pools, in which the organic materials are decomposed at different rates. The decay materials from these pools are then assigned to either slow or passive soil organic carbon pools. The base decomposition rate for each pool varies with temperature and moisture. Compared to the complex structures for the litter and soil carbon pools, its vegetation model and related processes have rather simple representation: three live carbon pools exist (leaf, wood, and fine root), with Ra assumed to be 50% of the photosynthetic assimilation (GPP). CASA' prognostically simulates LAI as a function of leaf carbon, SLA, and a phenology scheme based on *Dickinson et al.* [1998], but canopy height is not changed prognostically with the growth of woody carbon. Vegetation dynamics is not simulated by CASA'; thus the types and cover fractions of existing PFTs do not change from the initial conditions. All the state and flux variables in CASA' are updated with the CLM time step.

[15] CN is based on an ecosystem process model Biome-BGC version 4.1.2 [*Thornton et al.*, 2002; *Oleson et al.*, 2010; P. E. Thornton et al., Technical description of the Carbon and Nitrogen Cycle Model in the Community Land Model version 4, manuscript in preparation, 2011]. Biome-BGC was designed to study the terrestrial carbon, nitrogen, and water cycles under the influence of different climate, disturbance history, plant characteristics, and/or atmospheric chemistry. Its integration into CLM enables the model to simulate the interaction between carbon and nitrogen cycling, but vegetation dynamics is not included. The intimate relationships between nitrogen and plant ecophysiology are modeled in photosynthesis, respiration and allocation algorithms and also by detailed partitioning of vegetation into 20 carbon and 19 nitrogen pools. A model plant is composed mainly of leaf, fine roots, live stem, dead stem, live coarse roots, and dead coarse roots, but CN also considers so-called storage and transfer pools for each tissue. The carbon in the storage pool is extracted for maintenance respiration when NPP balance is negative, and the transfer pool provides a temporary storage of carbon for new tissue growth. Assimilated carbon is transferred first to these temporary storages and then to new growth, but with the added constraint of adhering to tissue-specific carbon:nitrogen stoichiometry. GPP allocation to each tissue follows allometric parameters (i.e., empirical ratios that describe relative size and growth of each plant tissue). Canopy height and LAI change as the mass of leaf and stem carbon changes. Leaf mass is converted to LAI by SLA, and CN has its unique representation of SLA as a function of the height of leaves within the canopy and sunlit/shaded conditions [*Thornton and Zimmermann*, 2007] in contrast to a single prescribed value for each PFT as in CASA' and DGVM. Other BGC pools include coarse woody debris, where it is assumed that only physical degradation occurs (i.e., no respiration flux into the atmosphere), and three litter pools that have different rates of decomposition. The decomposed litter products are moved sequentially from the fastest to the slowest of the three soil organic carbon pools. Disturbance by fire is included in the model and follows the approach by *Thonicke et al.* [2001], in which the probability of fire is computed as a function of air temperature and soil water content at each time step.

[16] The DGVM submodel, based on LPJ [*Sitch et al.*, 2003] and IBIS [*Foley et al.*, 1996; *Kucharik et al.*, 2000], focuses on large-scale vegetation dynamics among grass and tree PFTs [*Bonan et al.*, 2003; *Levis et al.*, 2004]. Shrub PFTs are excluded in CLM3.5-DGVM used in this study, but they will be included in the next version of CLM to allow for the shrub-grass-tree competition [*Zeng et al.*, 2008; *Oleson et al.*, 2010]. DGVM is thus distinguished from the previous two submodels because carbon cycling is dependent on the prognostic simulation of relative PFT abundances. The modeled processes causing population change are recruitment, natural fire, background and stress mortalities [*Levis et al.*, 2004]. The parameterization of natural fire follows the algorithm by *Thonicke et al.* [2001]. The mortality formulations depend mainly on temperature, but are indirectly related to water stress by preferred carbon allocation to root as well as by the elimination of a whole PFT population with a negative balance between its annual GPP and Ra. The number of individual trees is a prognostic variable, however, the carbon pools (leaf, fine root, sapwood, and heartwood) of each PFT represent an "average" of that PFT community since the distribution of age or height is not considered in the model. Those processes for vegetation dynamics and the update of vegetation biomass are computed on an annual timescale. Leaf mass is also updated annually, but leaf phenology is simulated daily by time-varying phenology factor that depends on temperature, photosynthetic productivity and leaf maintenance respiration. Allocation of photosynthate to plant tissues is based on allometric relationships and water stress, and the updated leaf and wood carbon pools determine LAI and canopy height, respectively. The representation of the litter and soil organic matter is not the main focus of DGVM and is simpler compared to CASA' and CN.

2.3. Model Setup and Driver Data

[17] We ran CLM3.5 offline (i.e., not coupled to an atmospheric model, thus without feedback from the land surface to the atmospheric conditions) and coupled individually to each of the three BGC models. The four model configurations are referred to hereafter as NoBGC (CLM3.5 not coupled to any biogeochemical models), CASA' (CLM3.5 coupled to CASA'), CN (CLM3.5 coupled to CN), and DGVM (CLM3.5 coupled to DGVM). The offline model simulation needs several atmospheric state and flux variables as well as time-invariant site-specific characteristics and parameters as summarized in Table 3. The soil texture values used in the simulations are 52% sand, 42% clay, and 6% silt, taken from LBA-Model Intercomparison Project (LBA-MIP) protocol version 3 (L. G. de Goncalves et al., The Large Scale Biosphere-Atmosphere Experiment in Amazônia, Model Intercomparison Project (LBA-MIP) protocol, version 3.0, obtained from http://www.climatemodeling.org/lba-mip/ on 20 June 2008). They are in the middle range between the clay- and sand-dominant end-members found in the work of *Silver et al.* [2000] and considered here to represent the "mean" texture of Tapajós National Forest including both the flux tower and TEE sites. The same soil texture is used in all the model soil layers since reported textures in other studies do not vary substantially for 1 m depth, and hydrologic parameters were found nearly constant with depth down to 10 m [*Bruno et al.*, 2006; *Belk et al.*, 2007]. The vegetation types and their frac-

Table 3. Summary of Model Input Data

Atmospheric Variables	Data Source or Values Used		
	Spin-Up	2000–2001	2002–2004
Downward solar radiation (W m^{-2})	*Qian et al.* [2006], 1948–1999	*Qian et al.* [2006]	*Stöckli et al.* [2008a]
Downward longwave radiation (W m^{-2})	-	-	*Stöckli et al.* [2008a]
Air temperature (K)	*Qian et al.* [2006], 1948–1999	*Qian et al.* [2006]	*Stöckli et al.* [2008a]
Specific humidity (kg kg^{-1})	*Qian et al.* [2006], 1948–1999	*Qian et al.* [2006]	*Stöckli et al.* [2008a]
Precipitation (mm s^{-1})	*Qian et al.* [2006], 1948–1999	*Qian et al.* [2006]	*Restrepo-Coupe* [2007]
Surface pressure (Pa)	*Qian et al.* [2006], 1948–1999	*Qian et al.* [2006]	*Stöckli et al.* [2008a]
Wind speed (m s^{-1})	*Qian et al.* [2006], 1948–1999	*Qian et al.* [2006]	*Stöckli et al.* [2008a]
Atmospheric CO_2 concentration (ppmv)	283–355	383	383
Nitrogen deposition (gN m^{-2} yr^{-1})	0.0688–0.4, *Randerson et al.* [2009]	0.4, *Markewitz et al.* [2004]	0.4, *Markewitz et al.* [2004]
Land Surface Variables[a]	Values	Data Source	
Vegetation type and fractional cover[b]	98% EBTT, 2% bare	L. G. de Goncalves et al. (The Large Scale Biosphere-Atmosphere Experiment in Amazônia, Model Intercomparison Project (LBA-MIP) protocol, version 3.0, obtained from http://www.climatemodeling.org/lba-mip/ on 20 June 2008)	
LAI (m^2 m^{-2})	*Stöckli et al.* [2008b] and L. G. de Goncalves et al. (The Large Scale Biosphere-Atmosphere Experiment in Amazônia, Model Intercomparison Project (LBA-MIP) protocol, version 3.0, obtained from http://www.climatemodeling.org/lba-mip/ on 20 June 2008)	*Stöckli et al.* [2008b] and L. G. de Goncalves et al. (The Large Scale Biosphere-Atmosphere Experiment in Amazônia, Model Intercomparison Project (LBA-MIP) protocol, version 3.0, obtained from http://www.climatemodeling.org/lba-mip/ on 20 June 2008)	
Canopy height (m)	35	L. G. de Goncalves et al. (The Large Scale Biosphere-Atmosphere Experiment in Amazônia, Model Intercomparison Project (LBA-MIP) protocol, version 3.0, obtained from http://www.climatemodeling.org/lba-mip/ on 20 June 2008)	
Soil texture	52% sand, 42% clay, 6% silt	*Silver et al.* [2000] and L. G. de Goncalves et al. (The Large Scale Biosphere-Atmosphere Experiment in Amazônia, Model Intercomparison Project (LBA-MIP) protocol, version 3.0, obtained from http://www.climatemodeling.org/lba-mip/ on 20 June 2008)	

[a]Some of the listed land surface variables are prognostically simulated by BGC models and not used; vegetation type and fractional cover are not applied to DGVM, LAI is applied only to NoBGC, and canopy height is not used by CN and DGVM.
[b]EBTT, Evergreen Broadleaf Tropical Tree; bare, bare ground.

tional covers are specified as 98% of tropical broadleaf evergreen trees and 2% of bare ground following those specified for KM67 tower for LBA-MIP, which are also close to 94% of canopy cover observed in the control plot of TEE site [*Nepstad and Mountinho*, 2008a]. The land cover for DGVM is given as 100% bare ground at the initial state, then it is prognostically simulated throughout the spin-up and evaluation (control and drought) simulations. The mean canopy height is set as a constant of 35 m for NoBGC and CASA'. Monthly values of LAI are given to NoBGC from LAI data assimilation by *Stöckli et al.* [2008b] and interpolated to daily values.

[18] Details on initial conditions and spin-up simulations are as follows. All applicable carbon and nitrogen pools were initialized to zero, and models were run until the slowest soil storage pools of water, carbon, and nitrogen had reached equilibrium, defined as monthly mean of the applicable state variable deviating less than 0.1% from the previous year. All three biogeochemical submodels required a significant spin-up period: 4000 years for CASA' and CN, and 1000 years for DGVM. Fifteen simulation years were enough for soil water to reach equilibrium for NoBGC. Three-hourly atmospheric forcing for the period 1948–1999 was extracted from a global data based on NCEP-NCAR reanalysis [*Qian et al.*, 2006] and used to drive the spin-up simulations by cycling the necessary number of times to achieve equilibrium. Because significant differences were

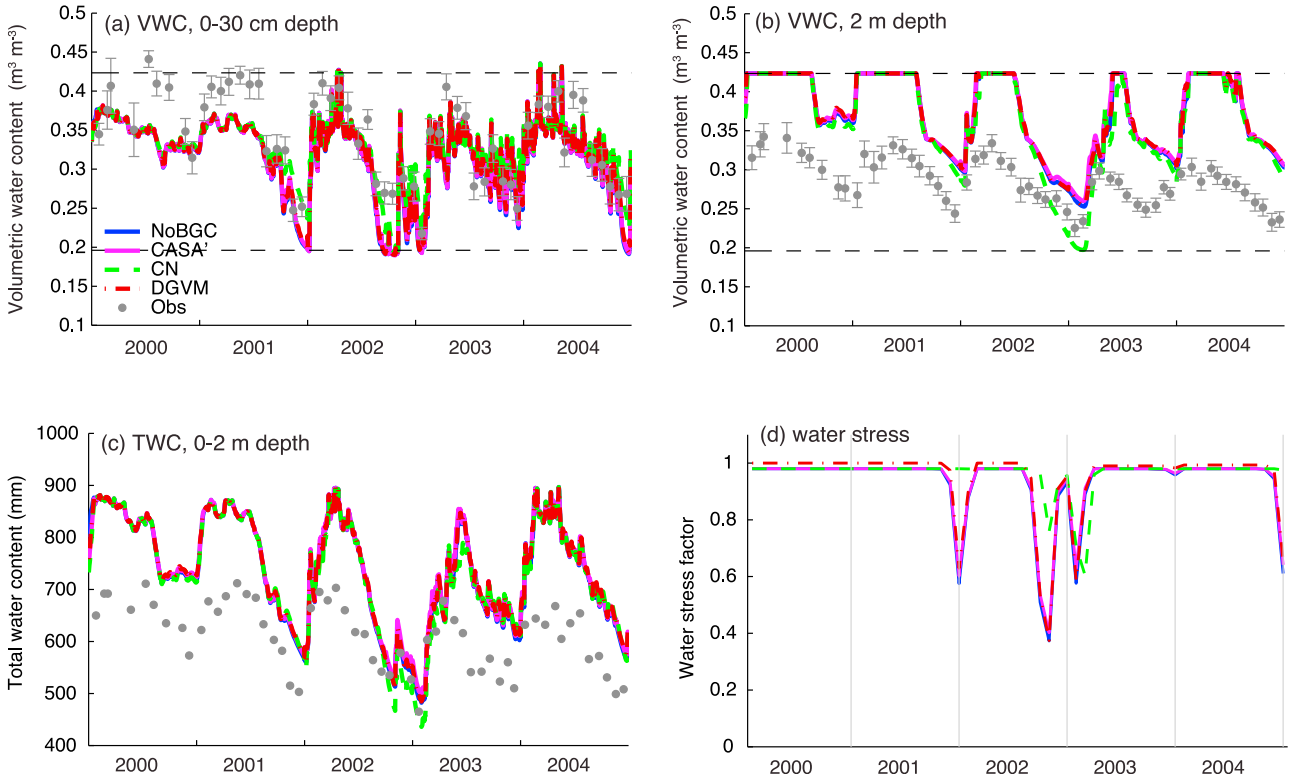

Figure 2. Soil moisture conditions. (a) Volumetric water content (VWC) from monthly in situ measurement at the control plot of the TEE Tapajos site (circles) and the daily means of model simulated values for 0–30 cm depth mean, (b) same as Figure 2a but for 2 m depth level, (c) 0–2 m total column soil water, and (d) water stress function (equation (A3)), which represents no water stress when its value is one, and severer water stresses as its value approaches zero. In Figures 2a and 2b, the upper and lower dashed lines represent the simulated saturated water content and wilting point, respectively.

found between the coarse resolution (grid resolution about 1.875°) global data and site-level eddy covariance measurements in the mean solar radiation, air temperature and specific humidity, the monthly mean differences in the three overlapping years (2002–2004) between the two data sets were applied as an offset to the *Qian et al.* [2006] data set in order to bring those data in the range of site-level measurements. For the spin-up simulations of the BGC models, atmospheric CO_2 concentration is held at preindustrial level of 283 ppmv. For CN, a climatological constant value of atmospheric deposition of nitrogen in the preindustrial condition (0.0688 gN m^{-2} yr^{-1}) is taken from the global nitrogen deposition data for Carbon-Land Model Intercomparison Project (C-LAMP) [*Randerson et al.*, 2009]. Then additional 100 year simulations were run to represent the twentieth century condition in which CO_2 concentration was gradually increased to reach 360 ppmv and nitrogen deposition gradually increased for CN to 0.4 gN m^{-2} yr^{-1} from *Markewitz et al.* [2004].

[19] Following the spin-up simulations, the control and drought simulations were run using the atmospheric forcing data from *Qian et al.* [2006] for the years 2000 and 2001, and these based on eddy covariance tower measurements [*Stöckli et al.*, 2008a] from the years 2002 to 2004. The precipitation in both data sets differ substantially from that reported by *Brando et al.* [2008], and was scaled by the monthly mean differences from *Brando et al.* [2008] (for 2000–2001) or replaced with the merged rain data by *Restrepo-Coupe* [2007] (for 2002–2004). The merged hourly precipitation time series was produced from the data at KM67, nearby KM83 flux tower, and Terra Rica rain gauge [*Nepstad et al.*, 2002]. Downward long wave radiation after *Stöckli et al.* [2008a] was high in comparison to nearby observations, and was modified such that the observed and simulated monthly mean diurnal cycles of net radiation agree with each other (with the Pearson correlation coefficient of 0.98 and the difference in standard deviation within 2% in both hourly and monthly timescales).

[20] In the drought treatment plot at TEE site, approximately 70% of the throughfall was diverted during the 6 months of the wet season from 2000 to 2004. This is simulated by modifying the canopy throughfall algorithm in CLM3.5. The canopy interception and throughfall (mm s^{-1}), q_{int} and q_{thru}, respectively, are computed in the model as follows [*Oleson et al.*, 2008];

$$f_{\text{int}} = 0.25\{1 - \exp[-0.5(LAI + SAI)]\} \quad (1)$$

$$q_{\text{int}} = f_{\text{int}}(q_{rain} + q_{snow}) \quad (2)$$

$$q_{thru} = (1 - f_{\text{int}})(q_{rain} + q_{snow}) \quad (3)$$

Table 4. Summary of the Statistical Comparison Between the Model Simulations and Eddy Covariance Observation[a]

	τ (kg m^{-1} s^{-2})		LE (W m^{-2})		H (W m^{-2})		NEE (μmol CO$_2$ m^{-2} s^{-1})		GPP (μmol CO$_2$ m^{-2} s^{-1})		Reco (μmol CO$_2$ m^{-2} s^{-1})	
Models	Hourly	Monthly	Hourly	Monthly	Hourly	Monthly	Hourly	Monthly	Hourly	Monthly	Hourly	Monthly
						Linear Correlation (r)						
NoBGC	0.85	0.79	0.92	0.67	0.74	0.49	-	-	0.90	*−0.19*	-	-
CASA'	0.85	0.79	0.92	0.64	0.75	0.50	0.90	*−0.13*	0.90	*−0.19*	*0.01*	*0.19*
CN	0.85	0.77	0.92	0.74	0.69	*0.05*	0.87	−0.38	0.90	*−0.28*	*0.00*	*0.02*
DGVM	0.85	0.77	0.91	0.64	0.75	0.57	0.89	−0.42	0.90	*−0.21*	*−0.01*	*−0.08*
						Normalized Standard Deviation (σ_n)[b]						
NoBGC	0.87	1.06	1.12	1.07	1.20	1.97	-	-	1.45	1.51	-	-
CASA'	0.86	1.12	1.07	1.04	1.20	2.05	0.67	0.48	1.37	1.39	4.33	1.38
CN	0.88	1.08	1.12	1.54	1.11	1.68	0.91	0.74	1.44	1.34	0.94	0.77
DGVM	0.59	0.56	1.11	0.95	1.18	1.89	1.01	0.94	1.35	1.30	2.04	0.40
						Root Mean Square Error (*RMSE*)						
NoBGC	0.08	0.02	57.33	18.53	44.97	12.44	-	-	7.92	3.45	-	-
CASA'	0.08	0.02	54.69	16.78	44.57	14.09	5.23	0.97	7.03	2.87	7.72	2.49
CN	0.08	0.02	58.74	21.31	45.50	11.63	5.29	1.16	7.69	3.23	2.40	1.17
DGVM	0.11	0.06	59.36	17.99	43.54	13.04	5.65	3.09	6.86	2.64	3.84	1.00
						Mean Bias Error (*MBE*)						
NoBGC	−0.01	−0.01	17.99	16.90	9.84	9.45	-	-	3.06	3.14	-	-
CASA'	−0.01	−0.01	15.87	14.86	11.77	11.35	−0.32	−0.32	2.46	2.53	2.12	2.19
CN	0.00	0.00	20.34	19.12	7.82	7.40	0.21	0.15	2.86	2.92	0.69	0.69
DGVM	−0.06	−0.06	18.14	16.38	10.71	10.81	−2.75	−2.80	2.23	2.29	−0.55	−0.54

[a]Here τ, momentum flux; LE, latent heat flux; H, sensible heat flux; NEE, net ecosystem exchange of CO_2; GPP, gross primary production; Reco, ecosystem respiration. The units are for RMSE error and MBE. The numbers in italic are not statistically significant with 95% confidence.
[b]The σ_n is obtained by normalizing (dividing) the simulated standard deviation (σ_m) by those from the observation (σ_o), i.e., $\sigma_n = \sigma_m/\sigma_o$.

where f_{int} is the intercepted fraction of the total precipitation, q_{rain} (mm s^{-1}) is the rainfall, q_{snow} is the snowfall (mm s^{-1}), LAI and SAI are the leaf and stem area index (m^2 m^{-2}), respectively. Equation (3) is modified for the drought experiment simulation as

$$q_{thru} = 0.3(1 - f_{\text{int}})(q_{rain} + q_{snow}) \quad (4)$$

so that 30% is retained in q_{thru}. The other 70% of the q_{thru} is added to surface runoff and is instantaneously removed from the system. The actual amount of the water reaching the ground is slightly higher than 30% due to stemflow, which remains unmodified. In addition, q_{thru} varies among different BGC model simulations due to the difference in prognostic LAI. The above treatment diverts a total of 630–960 mm of throughfall each year, similar to 620–890 mm as reported by *Nepstad et al.* [2007].

3. Results

3.1. Model Performance Under Natural Conditions

[21] Model performance is first assessed under natural conditions (utilizing standard, unmodified throughfall computation) in order to elucidate any model deficiencies before assessing these models' capability in simulating drought stress.

3.1.1. Soil Moisture

[22] The simulated volumetric water contents (VWC) (m^3 m^{-3}) by all the models agree fairly well with observation for the top 30 cm depth (Figure 2a). However, the modeled VWC progressively becomes higher than observed with depth (Figure 2b), leading to the overestimation of the total water content (TWC) (mm) of the top 2 m soil by 100–150 mm (Figure 2c). The simulated water table depth is much too shallow, ranging from ~0.5 m (wet season) to 2.8 m (dry season) while the typical depth in the Amazon basin is reported to be 5–15 m [*Costa et al.*, 2002] and it is exceptionally deep at ~100 m at the studied site [*Belk et al.*, 2007].

[23] A short-term intense drought in 2002 with consecutive months of less than 20 mm month^{-1} precipitation in August through October, and again in January 2003 after a brief recovery, reveals another model inconsistency between soil water content and vegetation activity. The modeled TWC agrees well with the observation in this period, but the simulated vegetation experiences significant water stress (Figure 2d and equation (A3)) while eddy covariance data does not show any noticeable water stress in this ecosystem as shown in sections 3.1.2–3.1.4.

[24] Some of the disagreement in the soil water content can be accounted for by the uncertainties in the forcing soil texture and empirical calculations for soil hydraulic parameters adopted in CLM3.5 [*Clapp and Hornberger*, 1978; *Cosby et al.*, 1984], but most disagreement is likely due to the modifications to soil hydrology with groundwater model in CLM3.5, as highlighted by *Zeng and Decker* [2009] and *Decker and Zeng* [2009]. We ran several sensitivity tests using different soil textures within the range of clay to sand end-members observed by *Silver et al.* [2000], but no particular texture could reproduce the observed soil moisture content both in dry and wet seasons. We did not further optimize hydrological parameters or soil textures because the saturated conductivity and soil porosity computed for the chosen texture by the empirical formulations (saturated conductivity = 5.76×10^{-3} mm s^{-1}, soil porosity = 0.42) are within the range estimated at the TEE site by *Belk et al.* [2007]. In a separate sensitivity test with a revised imple-

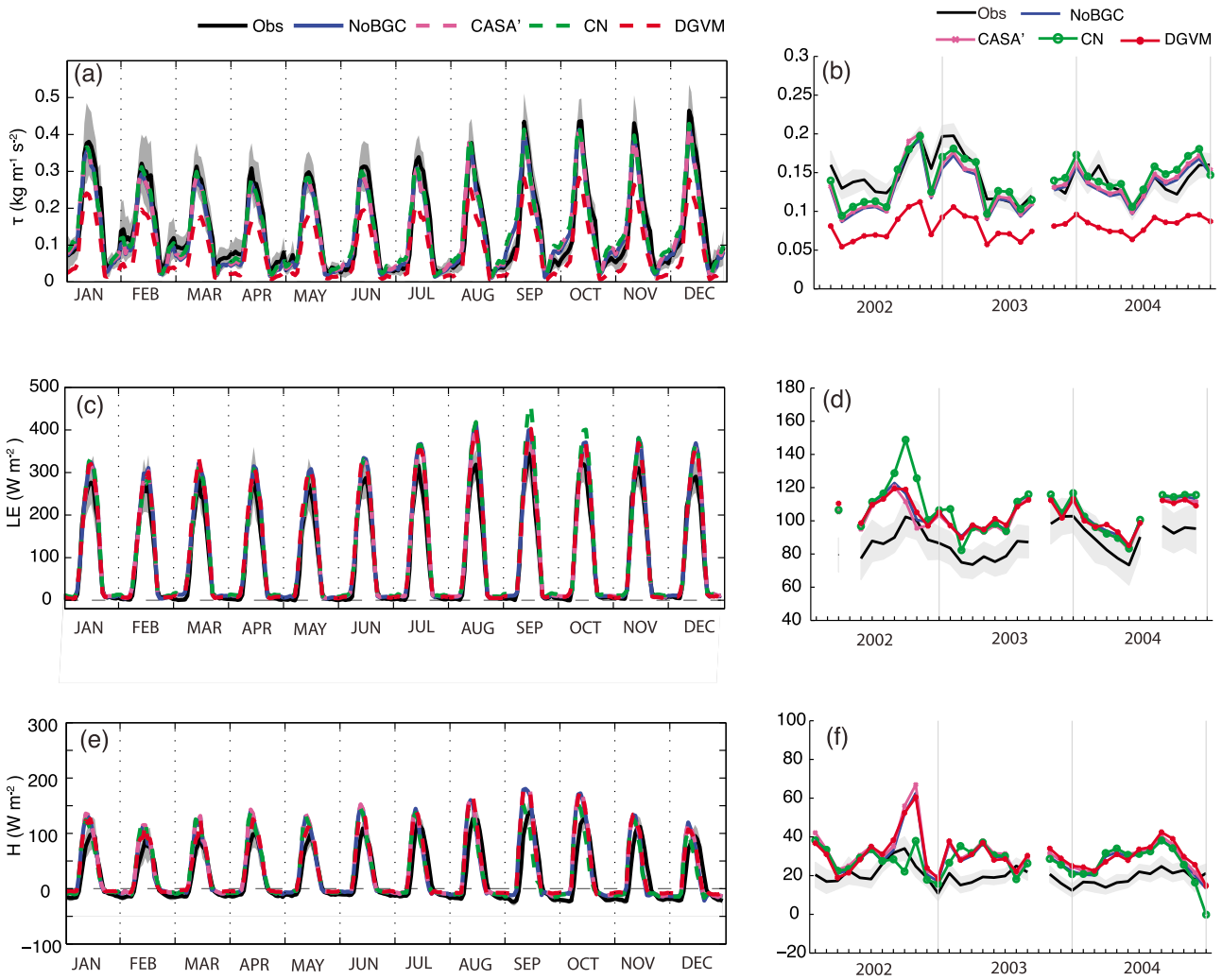

Figure 3. Observed and simulated fluxes. (a, b) Momentum, (c, d) latent heat, and (e, f) sensible heat. (left) Diurnal cycle for each month averaged over 3 years (2002–2004); (right) monthly mean time series for 2002–2004. Obs refers to the monthly mean computed from Brasil Flux data. Gray shading represents 95% confidence interval of the observed data, but does not include the uncertainties from the assumptions involved in the eddy covariance measurement or other systematic errors.

mentation of the Richards equation and bottom boundary conditions following *Decker and Zeng* [2009], the wet bias and the water table depth are significantly improved, however, the plant water stress is also strengthened. We focus on the results from the default CLM3.5 soil hydrology model in sections 3.1.2–3.1.4 because other model parameters relevant to this study have been calibrated for the default model.

3.1.2. Turbulent Fluxes: Momentum and Energy

[25] Model performance is evaluated by common statistical measures against the eddy covariance measurements; Pearson correlation coefficient (r), standard deviation normalized (divided) by the observed standard deviation (σ_n), Root Mean Square Error (RMSE), and Mean Bias Error (MBE) (Table 4). Overall, CLM3.5 well reproduces the diurnal and seasonal cycles of momentum exchange and energy balance, as well as the relative partitioning between LE and H components. All BGC submodels preserve this fidelity under natural conditions, with some exceptions analyzed below.

[26] In the diurnal cycle and monthly mean momentum flux, DGVM stands out as it underestimates the flux by 20–60% throughout the diurnal cycle, and by 40–70% of the monthly mean (Figures 3a and 3b, also discussed in section 3.1.4). The diurnal cycle of LE is reasonable in all simulations (good r and σ_n) but overestimation of the midday peak results in a positive monthly bias of 10–40 W m^{-2} (Figures 3c and 3d; see MBE, Table 4). H in this ecosystem is small and only 1/4–1/3 of LE, but MBE and RMSE are comparable to those for LE (Figures 3e and 3f). Well simulated seasonality in energy fluxes is disrupted by the short-term drought period from August 2002 to January 2003 when the simulated transpiration drops sharply because of the high water stress for vegetation, except for CN (section 3.1.1). The decrease in LE is balanced by the unrealistic positive peak in H. CN is the only model that can reproduce the observed energy flux tendency (albeit overestimating the magnitude of LE), because of its larger root mass distribution at deeper soil levels (Table 2 and

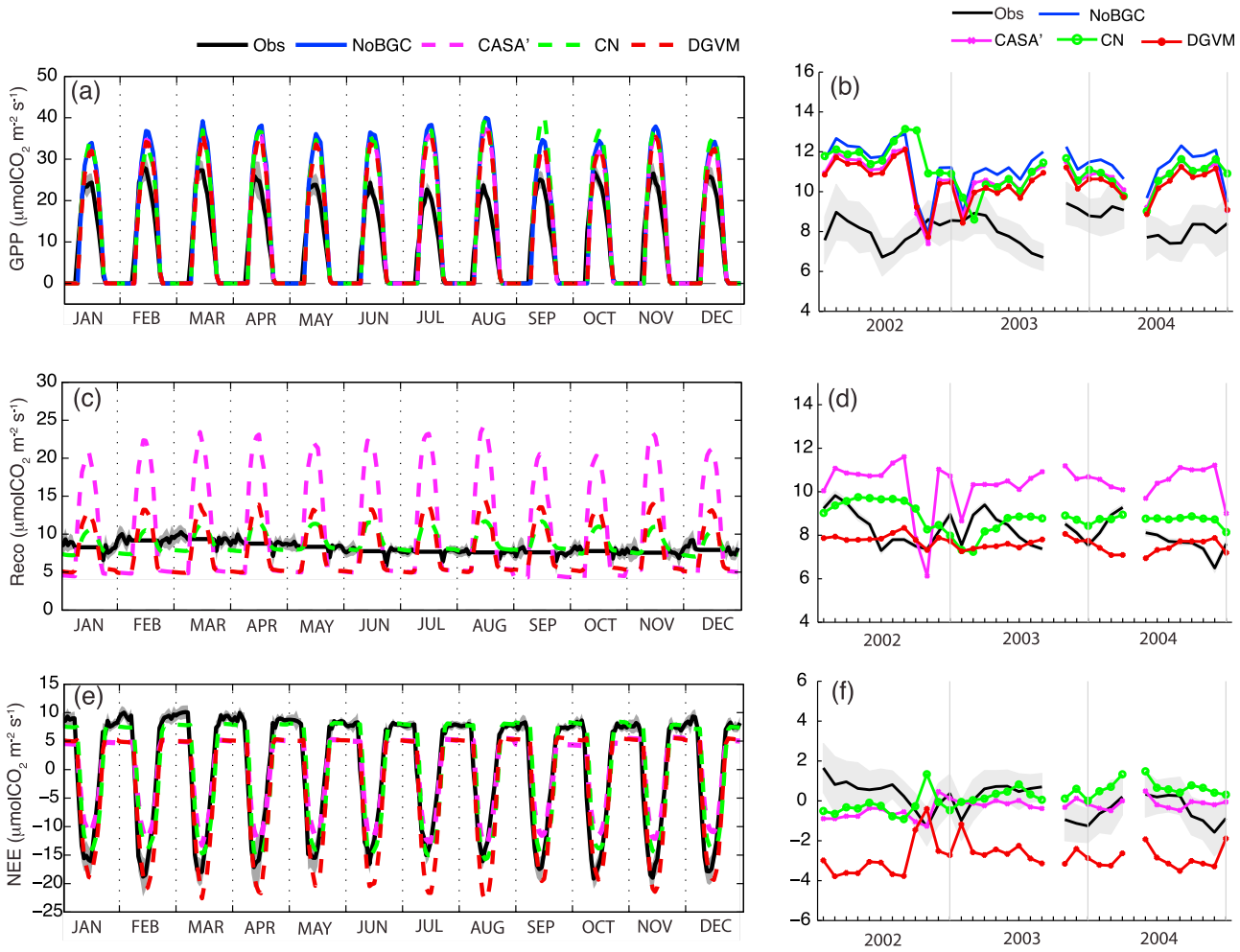

Figure 4. Same as Figure 3 except for observed and simulated carbon fluxes. (a, b) Gross primary production (GPP), (c, d) ecosystem respiration (Reco), and (e, f) net ecosystem exchange (NEE).

equations (A5) and (A6)). A caveat for the above analyses is that the uncertainty in the energy budget from the net radiation and eddy covariance measurements makes it less confident to assess models' systematic bias in LE and H (MBE and RMSE). However, the energy closure itself does not significantly depend on seasons, thus the eddy covariance data should be able to provide reliable evaluation of seasonality (r).

3.1.3. Carbon Fluxes

[27] Simulated hourly GPP shows high correlation (r = 0.9) with the eddy covariance measurements in all the model simulations, but σ_n suggests that its diurnal cycle is exaggerated by ~40% (Table 4). It clearly results from overestimating the midday GPP peak, which sometimes reaches a factor of two (Figure 4a). This overestimation of GPP is linked to that of LE because the stomatal resistance for water vapor transfer is inversely proportional to GPP in the model (equation (A1)), which emphasizes the importance of having realistic photosynthesis for energy and water cycles. Inter-model variation is small except for CN whose peaks of GPP in September and October are higher due to the smaller water stress than other models. In the monthly mean, simulated GPP stays well above the eddy covariance estimation by ~3 μmol CO_2 m^{-2} s^{-1} throughout the observed period (Figure 4b). There is also a mismatch between the modeled and observed seasonality. The modeled GPP increases throughout the wet season (January–July), reaches a maximum in the early dry season and drops in the later dry season, while the observed GPP decreases to its minimum early in the dry season and then gradually increases to the peak within the following wet season. The simulated seasonal cycle is much more responsive to the amount of rain, which also produces higher interannual variation than that observed.

[28] The temporal behavior of Reco is simulated poorly by all the models with statistically insignificant correlations and large RMSE and MBE (Table 4). For the monthly averaged diurnal cycle, the three BGC models simulate much higher diurnal peak values of Reco (Figure 4c) than that observed, partly due to the different assumptions about the temperature dependence of Reco between BGC models and the estimation based on eddy covariance data. We should also note that the estimation of Reco from NEE measured by eddy covariance method includes several other assumptions and associated uncertainties [*Baldocchi*, 2003; *Malhi et al.*, 2009b], which also affects GPP presented above. At the seasonal timescale, Reco is slightly higher in the wet season [*Hutyra et al.*, 2007] but this seasonal cycle of Reco is not captured by any of the models (Figure 4d).

Intermodel difference is large reflecting the differences in respiration algorithms (Appendix B).

[29] The combination of the exaggerated diurnal variation in GPP and Reco partly cancel each other, producing a high correlation with observed NEE diurnal cycles (r = 0.87–0.89; Figure 4e). However, the correlation with observations at the seasonal timescale is poor. The models tend to simulate either no seasonality or carbon uptake during the wet season and carbon loss in the dry season, which is opposite to the observed trend. DGVM simulations yield a too strong carbon sink during wet season, well outside the 95% confidence interval of the observed monthly mean NEE. A significant portion of this error comes from the overestimation of GPP by the new photosynthesis and soil hydrology models in CLM3.5, and the reasonable (dry season) and underestimated (wet season) Reco by DGVM does not cancel the GPP error as other models.

3.1.4. Vegetation Structure and Carbon Dynamics

[30] The growth of vegetation is determined by the balance between GPP and Ra, which are in turn affected by the size of the vegetation. The carbon captured in the plants is then transferred to dead carbon pools, another important system for carbon cycle. Those interactions make it important to evaluate the models on both the fluxes and storage sizes of carbon. For BGC models with dynamic vegetation, the types, number (stem) densities, and fractional coverage of PFTs are additional fundamental quantities to be evaluated.

[31] DGVM simulates the PFT competition as 95% broadleaf evergreen tropical tree and 5% C4 grass. It is reasonably close to the observed canopy cover, and while direct, quantitative comparison of PFT composition is not possible, year-round high (>5) values of LAI in this forest site indicate a dominance of the evergreen tree functional type. The stem density simulated by DGVM (629 stems ha^{-1}) is also difficult to compare to observations since the model represents the total number of trees with no size or age class distribution. The reported total stem density for trees and lianas with diameter at breast height (dbh) $\geq$ 10 cm and $\geq$ 5 cm, respectively, is 182–498 stems ha^{-1} [*Nepstad et al.*, 2002; *Rice et al.*, 2004], and we interpret that the simulation is probably in a reasonable range when the entire size distribution is accounted for.

[32] Aboveground Net Primary Production (ANPP, MgC ha^{-1} yr^{-1}) was estimated at the TEE site with annual stem growth measurements and litterfall data. Similar quantity is computed from the BGC models by annual integration of leaf and stem growth for each year, and their average and standard deviation throughout the 5 year period are compared to those from observation (Figure 5a). CASA' substantially overestimates the annual growth by a factor of three, but its interannual variation is reasonable. CN estimates ANPP reasonably with some overestimation on the mean value and standard deviation. DGVM overpredicts ANPP and particularly its year-to-year change.

[33] The disparities among the observed and simulated ANPP is translated into the wide range of the carbon storage size (Figure 5b and Table 5). Direct measurement of leaf biomass for the Tapajós Forest was not found, but it is roughly estimated to be 2.0~4.0 MgC ha^{-1} based on typical SLA [*Carswell et al.*, 2000; *Domingues et al.*, 2005; *Fyllas et al.*, 2009; *Nepstad and Mountinho*, 2009b] (also discussed below) and LAI values (5.8 m^2 m^{-2}) [*Nepstad and Mountinho*, 2008b; *Brando et al.*, 2010] found at this site and across the Amazon basin. It is slightly underestimated by CASA' (1.8 MgC ha^{-1}), reasonably simulated by CN (2.4–2.7 MgC ha^{-1}), and overestimated by DGVM (6.0–6.5 MgC ha^{-1}). The stem biomass is significantly overestimated by CASA' and CN as previously found by *Randerson et al.* [2009] while satisfactorily simulated by DGVM. However, exact comparisons of stem and root biomass are hindered by the lack of explicit representation of coarse root pool in CASA' and DGVM. Fine root carbon (1.7–2.1 MgC ha^{-1} [*Nepstad et al.*, 2002]) is reasonably simulated by CASA' (2.3 MgC ha^{-1}) and CN (2.6 MgC ha^{-1}), but overestimated by DGVM (7.8 MgC ha^{-1}). CN is the only model that has explicit live and dead coarse roots, but their simulated total size of 95.6 MgC ha^{-1} (live: 0.3 MgC ha^{-1}, dead: 95.3 MgC ha^{-1}) is quite larger than those obtained from the field study (15–16.5 MgC ha^{-1} [*Nepstad et al.*, 2002]). We note that the root biomass observation by *Nepstad et al.* [2002] is based on the surface to the depth of either 6 m (for fine root) or 12 m (for coarse root), much deeper than the modeled domain of 3.4 m, but this comparison is still meaningful since the majority of the root mass is typically concentrated near the surface [*Zeng*, 2001, and references therein]. It is also helpful to look at the relative proportion of each vegetation tissue (leaf, stem, fine and coarse roots) to assess the model bias in carbon allocation scheme (Figure 5c). The allocation to the fine root by CASA' and CN (0.4% and 0.6%, respectively) are both smaller than the number derived from the field data (1.2%, based on several references summarized by *Malhi et al.* [2009b]), while DGVM allocates higher fraction of 3.9%. The allocation to leaf is similarly smaller in CASA' and CN (0.3 and 0.6%, respectively) and larger in DGVM (3.1%) than observed (1.7%). CASA' and CN tend to transfer more carbon to tree trunk tissues (including coarse root) rather than leaf and fine roots, which actually helps to simulate reasonable leaf and fine root sizes with the overestimated GPP. Differences between the models and observation are also found in dead carbon pools. CASA' tends to overestimate coarse woody debris (CWD) and surface litter (76 and 6.6 MgC ha^{-1}, respectively), while its soil organic carbon (SOC) (109 MgC ha^{-1}) is about half of the observed size (220 MgC ha^{-1}). CN does not distinguish the above or below ground litter pools thus we added all the litter pools to the SOC pool for comparison, but it underestimates both CWD and SOC (29 and 69 MgC ha^{-1}, respectively). DGVM overestimates the surface litter (8.2 MgC ha^{-1}) whereas it underestimates SOC (78 MgC ha^{-1}). DGVM does not explicitly represent CWD, instead it is implicitly included in the stem heartwood and surface litter.

[34] Leaf biomass is converted to LAI, one of the key variables that couples biogeochemical processes to several biogeophysical processes. It is underestimated in CASA' and CN simulations as 4.4 m^2 m^{-2} and 3.5 m^2 m^{-2}, respectively, while DGVM significantly overestimates it as 14 m^2 m^{-2} (Figure 5d). For CASA' and DGVM, most of the disagreement is explained by the previously mentioned leaf mass. For CN, its prescribed SLA at the canopy top for the tropical evergreen broadleaf tree PFT (0.012 m^2 gC^{-1}) seems reasonable for Tapajós Forest (0.013 m^2 gC^{-1} [*Domingues et al.*, 2005]), but its canopy-average SLA values for sunlit leaves (0.013 m^2 gC^{-1}) and shaded leaves (0.015 m^2 gC^{-1}) are in the lower range found across the

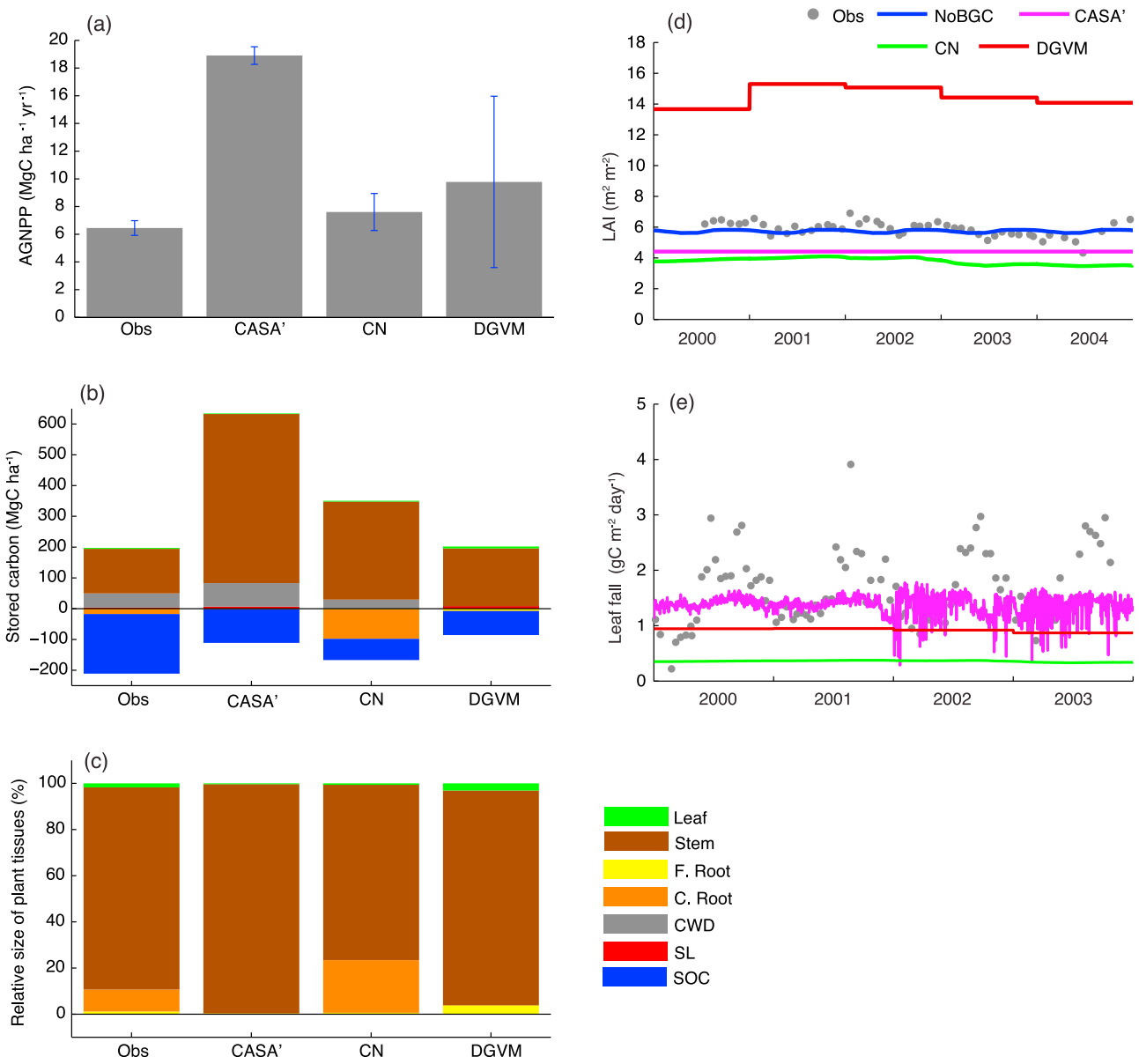

Figure 5. Comparison of observed and simulated carbon dynamics. (a) Mean annual above ground NPP and standard deviation (error bar), (b) carbon storage sizes, (c) relative proportion of carbon storage in the four vegetation tissues, (d) LAI time series, and (e) Leaf fall time series. Numerical values for Figure 5b are given in Table 5. In Figures 5a, 5d, and 5e, "Obs" refers to the field measurements at TEE Tapajós site control plot [*Brando et al.*, 2008; *Nepstad and Mountinho* 2008b; *Nepstad and Mountinho*, 2010]. In Figures 5b and 5c, "Obs" refers to the mean values from the compiled data by *Malhi et al.* [2009b]. The color legend for Figures 5b and 5c is given next to Figure 5c with the following notations: F. Root, fine root; C Root, coarse root; CWD, coarse woody debris; SL, surface litter; SOC, soil organic carbon. In Figure 5d, "NoBGC" represents the values used to force the model, not the simulated values.

Amazon forest (0.013–0.02 m^2 gC^{-1} and 0.02–0.04 m^2 gC^{-1} for sunlit and shaded leaves, respectively) [*Carswell et al.*, 2000; *Domingues et al.*, 2005; *Fyllas et al.*, 2009], probably leading to the underestimation of LAI with the rather reasonable leaf mass. It is also noticeable in Figure 5d that the simulated LAI has only year-to-year variations while the observed LAI time series exhibits small, but certain seasonality. The leaf carbon dynamics appears more clearly in the litterfall data, which shows distinct peaks every year in dry seasons (Figure 5e). Small variations in LAI and a distinct peak in litterfall indicate a period of leaf flush in the dry season [*Huete et al.*, 2006; *Doughty and Goulden*, 2008a; *Brando et al.*, 2010; N. Restrepo-Coupe, manuscript in preparation, 2011]. This leaf carbon dynamics is not captured by the three BGC models because leaf phenology (except for the background mortality) is not specified to the tropical evergreen broadleaf PFT. However, leaf turnover is suggested to be important in reproducing GPP seasonality at this

Table 5. Summary of the Observed and Simulated Ecosystem Properties[a]

Variables	*Nepstad et al.* [2002] Treatment	*Nepstad et al.* [2002] Control	*Rice et al.* [2004]	*Pyle et al.* [2008]	*Quesada et al.* [2009]	*Silver et al.* [2000]	*Malhi et al.* [2009b]	Model Simulations[b] CASA'	CN[c]	DGVM
Canopy height (m)	18~40	18~40	40 (mean)					-	36.0 (0.1)	20.6 (0.1)
LAGB[d] (MgC ha^{-1})	145.5	152.5	143.7 ± 5.4	148 ± 3				551.4 (1.2)	321.0 (2.0)	193.8 (2.2)
Fine root[e] (MgC ha^{-1})	1.7 ± 0.1	2.1 ± 0.2					30 ± 4	2.3 (0.0)	2.6 (0.1)	7.8 (0.5)
Coarse root[e] (MgC ha^{-1})	16.5 ± 3.4	15.0 ± 3.0					-	95.6 (0.6)	-	
Number of trees (ha^{-1})	182	203	469					-	-	632 (14)
CWD (MgC ha^{-1})			48 ± 5.2	43.9 ± 5.2				76.1 (0.6)	29.3 (1.8)	-
Surface litter (MgC ha^{-1})						3.75 ± 0.47		6.6 (0.1)	-	8.2 (4.5)
SOC[f] (MgC ha^{-1})					220			108.9 (0.1)	68.8 (0.5)	78.3 (1.9)

[a]Values from *Nepstad et al.* [2002] are converted from Mg biomass to MgC assuming that 50% of biomass is comprised by carbon. The values from *Rice et al.* [2004] and *Pyle et al.* [2008] were taken from the synthesis by *Malhi et al.* [2009b]. LAGB, live aboveground biomass; CWD, coarse woody debris; SOC, soil organic carbon.

[b]All the values from model simulations are mean values from 2000 to 2004 simulations. Values in parentheses are standard deviations for the 5 years based on monthly mean values.

[c]CN does not specify the physical locations (above or below ground) of the litter pools, thus the surface litter is not listed here. (Instead they are classified by the tissue types and decomposition rates: "labile," "cellulose," and "lignin.")

[d]For CASA', LAGB is obtained as the sum of the leaf and stem carbon; for CN it is the sum of leaf, live stem, and dead stem carbon; and for DGVM, it is the sum of leaf, sapwood, and heartwood carbon. The "dead" carbon pools within the stem are considered as part of the "live" biomass, to be consistent with the estimation in the field based on allometric equations [*Chambers et al.*, 2001a]. Unless the model results would provide unrealistically low values.

[e]Observed fine and coarse root biomasses in the work of *Nepstad et al.* [2002] are based on the depth range of 0–6.1 m and 0–12 m, respectively. The estimation of total root biomass by *Malhi et al.* [2009b] is for 0–1 m depth, and the values from the model represent the value for 0–3.43 m depth.

[f]The observation from *Quesada et al.* [2009] is taken from *Malhi et al.* [2009b] for three depth levels (0–1 m, 1–2 m, and 2–3 m) and summed to provide the total amount.

site due to the dependency of photosynthetic capacity on leaf age [*Doughty and Goulden*, 2008a].

[35] Canopy height is another variable that links biomass size to biogeophysical processes. The average canopy height in the Tapajós forest has been reported to be 35–40 m, although a recent LiDAR survey conducted in the area indicates a high variability (S. R. Saleska, unpublished data, 2010). Simulated canopy height by CN (36 m) agrees quite well with the observations while DGVM underestimates it at 21 m (Table 5). Canopy height produces a pronounced effect on the turbulent exchanges (especially for momentum and trace gases such as CO_2) in land-atmosphere coupled studies through its role in computing roughness length and zero-displacement height [e.g., *Oleson et al.*, 2004], and the underestimation of canopy height by DGVM leads to the low bias in the momentum flux (section 3.1.2). We should also note that the underestimation of the canopy height by DVGM is accompanied with the overestimation of stem biomass, suggesting that the generic allocation schemes in DGVM cannot simulate realistic structure for the tropical evergreen broadleaf PFT. A similar conclusion applies to CN with its overpredicted stem biomass.

[36] The above analyses are useful but should be considered to be first order for two reasons. First, direct data-model comparison is not always possible because the observed and simulated spatial domains are different (e.g., soil depth) or physical observation is not easily made (e.g., fractional cover of each PFT). Second, the exact disturbance history is not available, and thus not simulated in this study while the observed forest ecosystem is suggested to be recovering from past disturbances [*Saleska et al.*, 2003; *Rice et al.*, 2004].

3.2. Drought Scenario Simulations

3.2.1. TEE Simulation and Comparison

[37] Throughfall exclusion at the TEE site produced a significant difference in soil moisture throughout the observed depth (10 m), but we restrict our comparisons of the soil moisture to the data from the shallower layer (the top 2 m depth) since the model domain extends only to 3.4 m. The observation on the drought plot reported the TWC reduction of ~55 mm compared to the control plot after the first season of the exclusion treatment (Figures 2c and 6b). The difference increased to 98 mm in the third year and then stabilized at that level for the rest of the experimental period. This reduction for the first 3 years is reasonably reproduced in our model simulations, but the difference keeps increasing instead of stabilizing (Figure 6b). Although the models' wet bias still persists, especially during the wet seasons, the effect of the reduction in throughfall inputs appears in the simulated water stress function. As shown in the previous section 3.3.1, under natural throughfall it is only in the intense dry season of 2002 and part of the following wet season that the simulated vegetation experiences severe water limitation (Figure 2d), whereas water stress is imposed in every dry seasons after 2001 in TEE simulations (Figure 6c). Note that CN also simulates severe water stress regardless of the higher root fraction than other models in deep layers.

[38] In the field TEE experiment, the water stress appeared as the gradual decline of LAI from about 6 m^2 m^{-2} at the beginning of the experiment to less than 4 m^2 m^{-2} in the driest period of 2002, a 33% reduction (Figure 6d). CASA' does not show any drought stress on LAI; while DGVM simulates a decline, it remains unrealistically high. The simulated LAI response by CN is the most realistic, with a

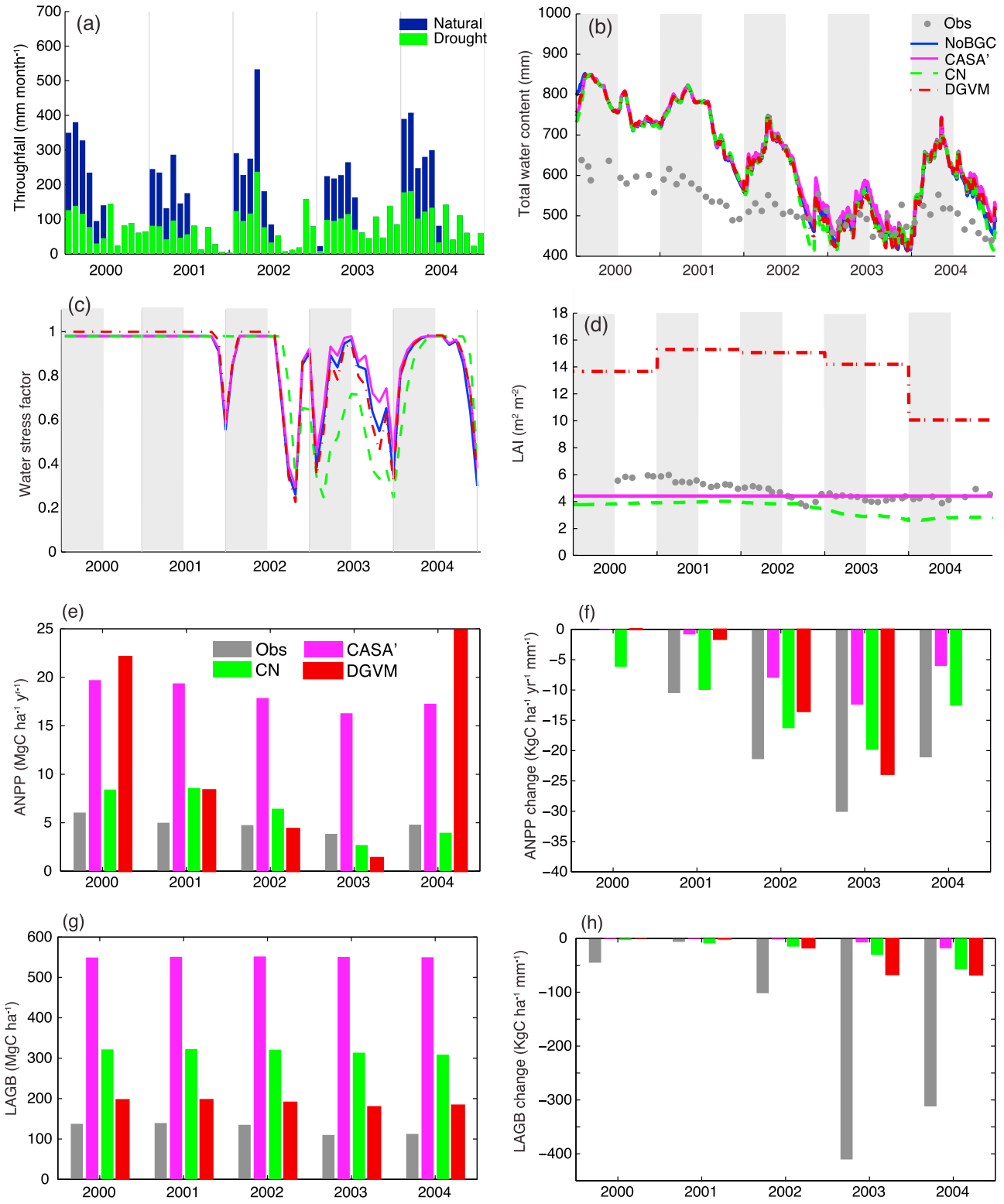

Figure 6. Results from the throughfall exclusion simulations. (a) Throughfall in the natural and drought simulations by NoBGC model, (b) 0–2 m total soil water (TSW), (c) water stress function (equation (A3)), (d) LAI, (e) observed and simulated above ground NPP (ANPP), (f) difference in ANPPs from the drought and control experiments, normalized by TSW difference (equation (5)), (g) Live Above Ground Biomass (LAGB), and (h) difference in LAGB between the drought and control experiments, normalized similarly to Figure 6f. Gray shading in Figures 6b–6d represents the period of throughfall exclusion (i.e., typical wet season).

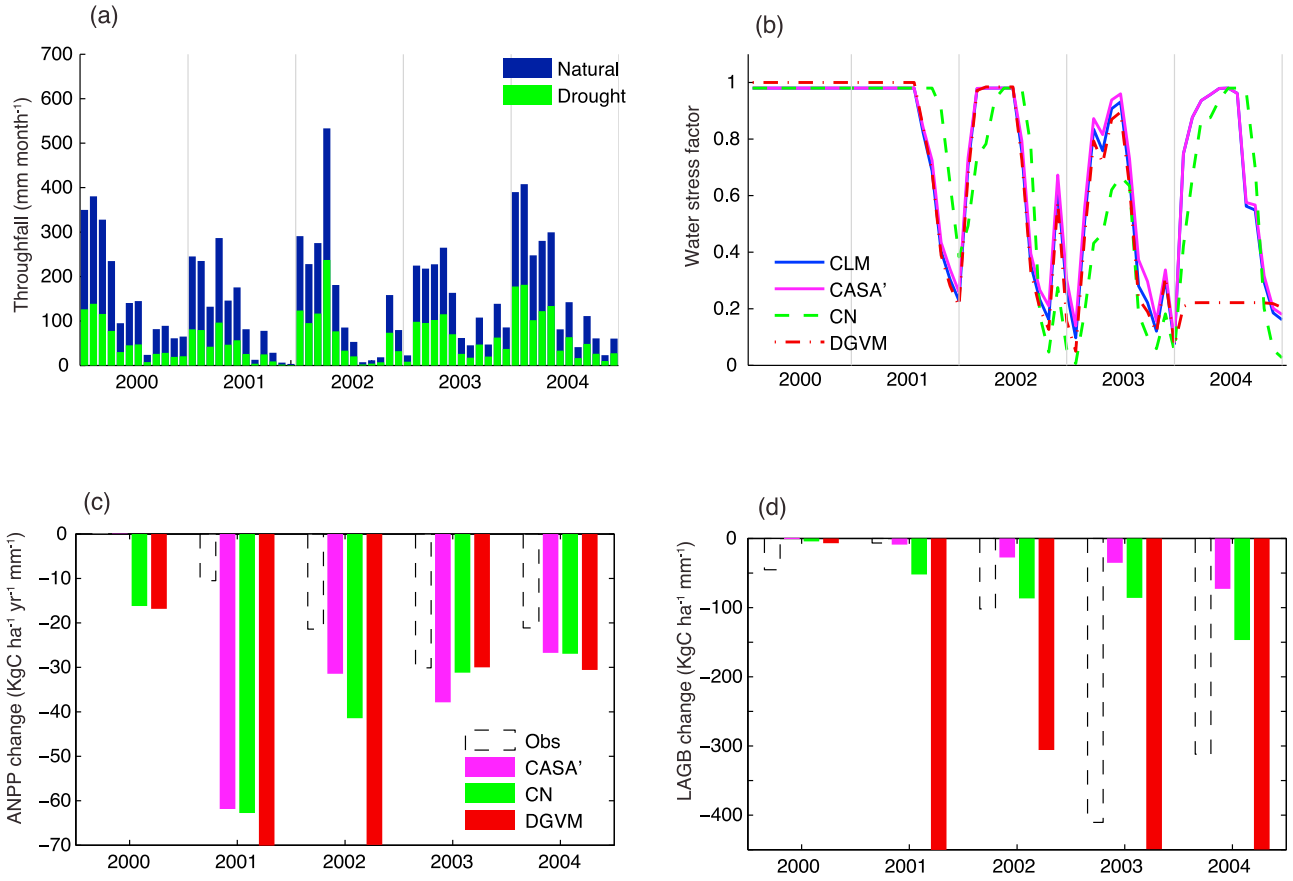

Figure 7. Main results from the all-year drought simulations. (a) Monthly throughfall in control (blue) and drought simulations (green), (b) water stress function (equation (A3)), (c) normalized difference in ANPP (equation (5)) between the all-year drought and control simulations, and (d) normalized difference in LAGB. In Figures 7c and 7d, the bar graphs with dashed lines represent the reduction levels observed in the wet season throughfall exclusion experiment [*Brando et al.*, 2008], as a reference.

reduction of 20–40% from the control simulation, but the timing of the decline is delayed by almost 2 years.

[39] For the drought response in ANPP, progressive decline in each year and slight recovery in the wetter year (2004) was observed in the field (Figure 6e). Although all the BGC models clearly overpredict ANPP, the overall yearly behavior of ANPP is reproduced except for DGVM. The ANPP sensitivity to drought in DGVM simulation is not realistic; it drops by more than 90% from the first to the fourth year and recovers in the following year to reach 45 MgC ha^{-1} yr^{-1}, even higher than that in the control simulation. This drastic response is likely caused by the DGVM allocation scheme in which the computation of growth (positive NPP) and mortality (negative NPP) are coupled and constrained by the allometic relationship; the stem biomass has a negative ANPP (i.e., mortality) in year 2003 when all the available assimilated carbon is used for root and leaf growth, and the new root and leaf biomass (growth minus background mortality) is still not large enough to sustain the current stem biomass according to the allometric relationship. In the following wetter year, the stem biomass is quickly increased to satisfy the allometric relationship with new and larger leaf and root biomass, resulting in an unrealistic stem growth.

[40] When ANPP is compared to the control field experiment, the observed ANPP reduction was 12% (2001), 30% (2002), and reached the largest 41% in the fourth year (2003). ANPP by CASA' is the least sensitive to drought, with the ANPP reduction being at most 13% relative to the control simulation. CN overestimates the largest ANPP drop in 2003 as 57%, although its prediction stays the most reasonable among the models. The largest change simulated by DGVM amounts to be 78% reduction, nearly twice the observed. This simple comparison of the simulated and observed ANPP reduction, however, may be affected by the models' biased soil moisture. Thus the sensitivity of ANPP to drought is also evaluated by normalized change of ANPP using the respective modeled reductions in TWC;

$$\Delta ANPP_{norm} = \frac{ANPP_{TEE} - ANPP_{CTR}}{\langle TWC_{TEE} \rangle - \langle TWC_{CTR} \rangle} \tag{5}$$

where $\Delta ANPP_{norm}$ is the normalized change of ANPP, $\langle TWC \rangle$ is the annual mean of the total water content (mm) in the top 2 m depth, and the subscripts CTR and TEE refer to the natural and drought experiments, respectively. The normalized ANPP change reveals that the modeled ANPP responses in CN and DGVM simulations are not overestimatetion,

instead it is rather smaller than the observed level when considered per unit change of soil water content (Figure 6f). Therefore these models may underestimate the change of ANPP due to drought stress, given unbiased soil moisture.

[41] The simulated sensitivity of live aboveground biomass (LAGB) to drought stress is substantially smaller than the observed (Figure 6g). *Brando et al.* [2008] observed that the most intense drought impact on LAGB was the loss of ~30 MgC ha^{-1} yr^{-1} relative to the control experiment in the last 2 years. On the contrary, the modeled decline was only ~10 MgC ha^{-1} yr^{-1} or less. This discrepancy is further enhanced when the loss of LAGB is normalized similarly to ANPP (Figure 6h). In the fourth year, the normalized difference of LAGB on the observation is about 400 kgC ha^{-1} mm^{-1}, while the predictions by all the models are less than 70 kgC ha^{-1} mm^{-1}. The main reason for the insensitivity of the modeled LAGB is that CASA' and CN do not have explicit mortality mechanisms from water stress for tropical evergreen PFT, thus LAGB experiences only a background mortality. The drought mortality is included in DGVM in the allocation algorithm as negative allocation to the plant tissue, but it is not large enough to reproduce the loss of LAGB at the observed level. It also can produce unrealistic ANPP response as described above.

[42] The total stem density in DGVM simulation remains the same between the control and drought simulations in the first 3 years, followed by a small reduction of 17 stems ha^{-1} (3%) in the fourth year. It appears to be within a reasonable range comparing with the 3–7% increase in the mortality observed in the field experiment [*Nepstad et al.*, 2007; *Brando et al.*, 2008], but lack of size structure in DGVM prohibits direct comparison of stem mortality from the TEE field study (as defined by *Nepstad et al.* [2007]). We also note that the modeled stem density is quite sensitive to precipitation such that it can remain the same or even slightly increase in similar drought simulations, depending on precipitation inputs varying within a reasonable climatological range. For PFT relative abundance, small shifts (~3%) favoring C4 grasses were simulated, presumably unsupported by data.

3.2.2. Sensitivity Tests Under Different Drought Scenarios

[43] We conducted additional sensitivity tests to further understand the model behavior by finding in which season or how much throughfall exclusion is necessary for the models to produce a LAGB response similar to that observed. In one experiment where throughfall reduction is imposed during the dry season instead of the wet season, the simulated drought response of LAGB is even less than that for the wet season exclusion (not shown). In another experiment, throughfall exclusion is applied throughout the entire year (Figure 7a). The associated intensification of water stress in the model caused the greater reduction of ANPP, but the normalized reduction of LAGB by CASA' and CN is still smaller than the observed loss in wet season only TEE (Figures 7b–7d). DGVM predicts a catastrophic die-off of the tropical evergreen PFT after the fourth year, resulting in a loss of the entire LAGB of the PFT. 95% of the grid area is replaced with C4 grass within 2 years. This is unlikely to take place in the real world, considering the results from another TEE in eastern Amazon forest where 7 years of year-round throughfall exclusion yielded 2.5% yr^{-1} mortality on average [*da Costa et al.*, 2010], and is reflective of limitations of DGVM associated with its primary purpose to represent global-scale plant biogeography (see biogeographical rules in section 2.2). Together with a separate offline simulation in which throughfall was brought back to the control level, it highlights an important tipping point: 20 years were required to recover a dominance of evergreen forest.

4. Discussion

4.1. Photosynthesis and Respiration

[44] CLM3.5 and its BGC submodels are shown to significantly overestimate photosynthesis. Overly wet soil causes some overestimation, but we found persistent high photosynthesis in other offline simulations with more realistic soil water content following the approach of *Decker and Zeng* [2009]. An analysis of photosynthesis–light response curve reveals a light saturation of photosynthesis around 30 $\mu molCO_2$ m^{-2} s^{-1} for this forest while modeled photosynthesis lacks any such asymptote (Figures 8a and 8b). A similar disagreement in the asymptotic behavior is also found in the relationship between photosynthesis and ecosystem ET (not shown), together suggesting that other factors (temperature, diurnal water stress, or nutrients) are limiting midday ecosystem photosynthesis. One hypothesis explicitly incorporated in the CN's nitrogen limitation model is that nutrient limitation constrains assimilation (section 2.2), which brings in the modeled light use efficiency (LUE, defined here as the initial slope of GPP–photosynthetically active radiation relationship) in much closer agreement with observations (Figure 8c), but the existence of other midday limiting factors are also possible [see *Doughty et al.*, 2006]. Another potential cause for discrepancy in observed versus modeled LUE, posing a challenge for further development of BGC models, is in scaling of photosynthesis from the leaf to the canopy. It is known that the size structure of the forest influences light penetration and diffuse/direct light environments, but the current model is lack of size structure or parameterizations for the effect of forest gaps [e.g., *Watanabe et al.*, 2002; *Fisher et al.*, 2010]. Further, the parameters for the linearly varying SLA within the canopy profile were verified with temperate forests [*Thornton and Zimmermann*, 2007], but may need to be evaluated with data from tropical forests [e.g., *Carswell et al.*, 2000; *Domingues et al.*, 2005].

[45] Respiration is another key part of the carbon balance in which our analysis revealed considerable disagreements among the models, each of them also differing from the eddy covariance estimation. For example, the diurnal range of Reco is quite large in all the three BGC simulations, mostly due to strong temperature effects on plant respiration (Ra). CASA' assumes that Ra is 50% of GPP, which is generally supported for temperate forests and also for Tapajós forest [*Delucia et al.*, 2007; *Malhi et al.*, 2009b], but this assumption produces the largest diurnal cycle of Reco that is in poor agreement with observations. This simple Ra calculation seems unrealistic for models with subdaily time steps and for the Amazon forest where only 30% of GPP is typically used for biomass growth [*Chambers et al.*, 2004; *Malhi et al.*, 2009b]. The temperature sensitivities of Ra and Rh are represented by either a Q_{10} (CN) or Lloyd-Taylor function (DGVM) (equations (B2), (B6), and (B11)), but their accuracy has been shown to be poor particularly at temperature

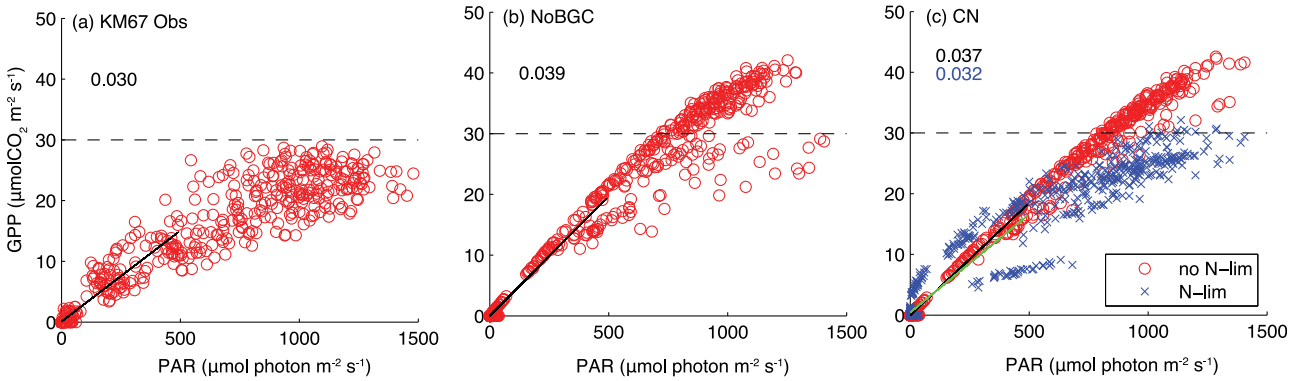

Figure 8. Observed and modeled relationship between GPP and photosynthetically active radiation (PAR) based on the monthly averaged diurnal cycles in 2002–2004. (a) Observation from the eddy covariance tower, (b) CLM3.5 without BGC models (NoBGC), and (c) CN "no N-lim" and "N-lim" are based on GPP computed without and with nitrogen limitation, respectively. The number in the top left corner of each panel is the initial slope of the linear-fitting curve. The horizontal dashed lines represent the apparent maximum GPP in the eddy covariance data. The results from CASA' and DGVM are almost identical to those from NoBGC and hence are not shown.

above 20°C [*Atkin et al.*, 2005; *Davidson et al.*, 2006], which is common in the Amazon forest. Recent observational studies provide hints for more process-based parameterizations that distinguish "apparent" temperature sensitivity [*Davidson et al.*, 2006], but such fully mechanistic representation of fine-scale processes, including the diffusion of gas and substrate through the air or water, may not be feasible yet to be incorporated in the current BGC models. A simpler representation still should follow general functional behaviors and spatial variations in parameters [e.g., *Khomik et al.*, 2009; *Zhou et al.*, 2009].

[46] Realistic partitioning and appropriate treatment of distinct carbon pools are also important for simulating respiration fluxes. Since each pool (e.g., leaf, surface litter, or slow soil carbon) has distinct physical and chemical characteristics, environmental conditions, and the rate of respiration per unit carbon (k_i in equations (B1) and (B7), and r_{resp} in equation (B10)) [*Chambers et al.*, 2004]. Therefore a lumped representation of multiple carbon pools has more difficulty in simulating the timing and magnitude of respiration response to the changing environment. For example, soil moisture is currently used for adjusting the decomposition rate of aboveground litter in CASA' and DGVM, but it is observed that the aboveground litter dries more quickly than soil, leading to different seasonality between the aboveground and belowground carbon pools [*Chambers et al.*, 2001b; *Sotta et al.*, 2007]. Table 6 compares the observed and simulated mean respiration fluxes and the residence time (storage size divided by flux) of different carbon pools to better illustrate the relationship between the carbon storage size and the respiration flux. One can see that the timescale of carbon flow through vegetation (Ra) in CASA' and dead carbon pools (Rh) in all the models are not in good agreement with the observation. These differences will be reflected in atmospheric CO_2 concentration and resulting radiative forcing in a fully coupled simulation. Such partitioned measurements of storage sizes and respiration flux is quite valuable to constrain the strength and weakness of the respiration algorithms and their optimizations, but models need to have realistic representation of carbon pools that can be directly compared to the data in order to take advantage of those measurements. At the same time, the difficulty in further partitioning in field measurements still hampers complete analyses. For instance, our residence time analysis for the stem in CN and DGVM is not quite comparable to the observation because the dead portion of the stem and coarse root is included in the observed biomass while it does not take part in the respiration flux.

4.2. Water Stress and Mortality

[47] Our analysis found that the water stress for photosynthesis (equation (A3)) is simulated too severely by the base model CLM3.5, while the reduction of LAGB is underestimated by all the BGC models. The former is the response to short-term drought and/or regular dry period, and the latter is the response for a long-term drought. In a short-term drought in the studied ecosystem, CLM3.5 fails to simulate the observed GPP seasonality. Previous versions of CLM and other land surface and ecological models had the same problem [*Saleska et al.*, 2003], and this study showed that reasonably or even overly wet soil with explicit consideration of groundwater in CLM3.5 does not fully reproduce the interactions between soil water and tropical vegetation. Instead, it is necessary to review tropical tree PFT parameters [e.g., *Domingues et al.*, 2005], reformulate the water stress function [e.g., *Fisher et al.*, 2010], or include biophysical processes found in the same or similar ecosystems such as deep root systems [*Bruno et al.*, 2006] and hydraulic redistribution [*Oliveira et al.*, 2005]. Some of these have already been tested by *Lee et al.* [2005] and *Baker et al.* [2008] with promising results. Incorporation of a more mechanistic representation of the soil-to-leaf continuum [*Sperry et al.*, 1998; *Fisher et al.*, 2006, 2007] with parameters for root architecture and the relative contributions of soil, root, and xylem hydraulic resistances to water transport, instead of a single water stress function solely dependent on soil water content, is a possible next step for a more mechanistic basis of drought-induced stress.

[48] The modeled mortality (LAGB loss) from the long-term drought is substantially less than the observed. One

Table 6. Comparison of Average Respiration Fluxes and Residence Time[a]

	Synthesis From in Situ Measurements				Model Simulations					
	Tapajós		Three Forests Mean		CASA'		CN[b]		DGVM[c]	
Respiration Components	Respiration (MgC ha^{-1} yr^{-1})	Residence Time (years)	Respiration (MgC ha^{-1} yr^{-1})	Residence Time (years)	Respiration (MgC ha^{-1} yr^{-1})	Residence Time (years)	Respiration (MgC ha^{-1} yr^{-1})	Residence Time (years)	Respiration (MgC ha^{-1} yr^{-1})	Residence Time (years)
Leaf	7.4 ± 4.0	0.4	8.8 (1.3)	0.3	-	-	10.3 (0.7)	0.3	8.8 (0.5)	0.7
Stem	3.8 ± 1.0	39	4.4 (0.7)	39	-	-	4.0 (0.5)	80	9.0 (0.5)	21
Root[d]	3.7 ± 0.8	5.9	5.6 (1.9)	6.2	-	-	8.6 (0.6)	0.3	10.5 (0.5)	0.7
Autotrophic total	14.9 ± 4.2	12	18.7 (3.4)	11	20.5 (1.9)	27	23.1 (1.7)	14	28.3 (1.5)	7.1
CWD	4.5 ± 1.1	9.8	3.1 (1.3)	7.8	6.3 (0.6)	12	-	-	-	-
Heterotrophic	14.9 ± 1.4	13	11.3 (3.1)	15.5	19.3 (1.9)	6.0	11.0 (1.8)	6.3	0.3 (0.1)	288
Ground based total	29.8 ± 4.4	14.0	29.7 (0.4)	13.7	39.8 (3.6)	19	34.2 (2.2)	12	28.6 (1.5)	10
Flux tower total	32.5 ± 0.4	12.8	30.5 (2.8)	13.3						
Soil	12.0 ± 0.6	18.0	12.5 (0.8)	16.5	13.0 (1.3)	8.6	19.2 (1.8)	-	10.7 (0.5)	8.0

[a]Residence time is obtained by carbon storage divided by flux. In situ estimation is taken from the synthesis by *Malhi et al.* [2009b] for three forest sites: Manaus, Tapajós, and Caxiuanã. For Tapajós Forest the uncertainty is given as the standard error for 95% confidence, computed following the method of *Malhi et al.* [2009b] with equal weight for each available data. The values in parenthesis are standard deviations, either among the three forests or from the monthly mean values from the simulations. Ra, autotrophic respiration (=Rleaf + Rstem + Rroot); CWD, coarse woody debris; Rh, heterotrophic respiration; Reco, ecosystem respiration (=Ra + R_{CWD} + Rh); Rsoil, soil respiration (=Rroot + Rh).
[b]CN has coarse woody debris pool, but it is assumed that there is no direct CO_2 emission to the atmosphere from it.
[c]Growth respiration in DGVM is computed as a single value for a whole plant. They are equally divided (by 3) and added into leaf, stem, and root respirations.
[d]The residence time of root carbon from the in situ data is obtained from the estimated root respiration and total root biomass, which likely includes the unknown amount of dead tissue within the coarse root. The residence time is computed for live tissues only from the model simulations (fine and coarse roots for CN, and fine root for DGVM).

approach for more realistic simulations is to relate the water stress function for photosynthesis to plant mortality as a first-order representation of hydraulic failure and/or insufficient photosynthesis for metabolism, thus coupling the plant responses for short-term and long-term drought. It is incorporated in DGVM but results in unrealistic ANPP response under drought scenario, probably because of its inappropriate way of coupling to the allocation algorithms. In addition, such a mechanistic approach needs to be combined with the size structure to address relevant mechanisms responsible for an interesting finding of the TEE field study in which stem mortality varied with size class. *Nepstad et al.* [2007] reported that for small size class (diameter from 2 to 5 cm dbh) there was no significant differences in the mortality between the control and throughfall exclusion plots, while almost twice higher mortality for medium size class (10–30 cm dbh), and more than fourfold higher mortality among the largest size class (>30 cm dbh) were observed. We further note that in the BGC models tested here, there is no link between the root biomass and plant's ability to take water from the soil. Therefore, even though there are significant differences in the simulated root biomass among the three BGC models, these differences do not translate into differences in the predicted water stress.

[49] Another drawback of the models without size class is the difficulty in properly simulating the resource availability and competition following the mortality of large individuals [*Smith et al.*, 2001; *Moorcroft*, 2006]. Considerable difference in the results between the "average individual" and "size class" models in the Amazon forest were illustrated by *Huntingford et al.* [2008]. They compared off-line simulations for future Amazon forest by TRIFFID DGVM [*Cox*, 2001] which uses similar approach as the three BGC models in this study, to those of the Ecosystem Demography (ED) model which incorporates a statistical approximation for size structure [*Moorcroft et al.*, 2001]. In both simulations forest biomass in the Amazon was substantially reduced by year 2100, but vegetation carbon loss simulated by ED model was about half of that by TRIFFID model [see *Huntingford et al.*, 2008, Figures 1c and 3]. Global implementation of models similar to ED may be still difficult, and most of their applications have been for regional and local scales [*Smith et al.*, 2001; *Huan et al.*, 2008; *Medvigy et al.*, 2009; *Fisher et al.*, 2010]. However, model intercomparisons of the above two model groups in regional model simulations can be valuable inputs for better parameterizations of global-scale BGC models.

5. Conclusion

[50] CLM3.5 incorporates improved soil hydrology and biogeophysical parameterizations to reduce the bias in energy and water cycles in the previous version. Our evaluation of its performance with various in situ measurements revealed that under the natural conditions, the biogeophysical aspects of the land-atmosphere interactions such as momentum and energy exchanges are reasonably simulated, but the water stress for photosynthesis from a short-term, naturally occurring drought condition is much exaggerated, and it degrades the model fidelity in the seasonality of energy fluxes. It is also found that the modeled controls on maximum photosynthesis are inconsistent with the field observation and allows the

model vegetation to have unrealistically high net productivity. The models show more difficulties to agree with the observations in biogeochemical processes, as highlighted by statistically insignificant correlations in the seasonal cycle of NEE, highly overestimated LAGB, and inconsistent relationships in the carbon pool sizes and the respiration fluxes. Similar results by *Randerson et al.* [2009] implicates that the errors from model parameterizations exceed those from global-scale input data. Further review on the characteristics of tropical tree PFTs, allocation algorithms and more realistic model representation of carbon pools are necessary.

[51] In the model experiments under long-term artificial drought conditions, the sensitivity of ANPP to drought stress is reproduced by the BGC models to some extent, but the drought sensitivity of aboveground biomass pools (including LAI) is grossly underestimated. It questions the reliability of future projections of the Amazon forest dieback when these BGC models are coupled to general circulation models, and suggests the need for the enhancement of mortality processes in the model as well as for the field measurements targeting specific mechanisms for mortality. Some of the processes responsible for the observed drought-induced mortality depend on the size-class structure, which are not readily incorporated in global BGC models yet, particularly taking into consideration the long timescale needed for BGC simulations. We speculate that intercomparison of large-scale and fine-scale BGC models [*Smith et al.*, 2001; *Huntingford et al.*, 2008] would provide hints for the improvements of the current parameterizations or size-class representations adoptable for global-scale models. It is also possible to improve the model's realism by linking the existing, but uncoupled processes; the root biomass and water stress for photosynthesis, and this water stress accumulated into plant mortality.

[52] We realize that our analysis do not provide the uncertainties of the simulation results that are caused by the errors in the forcing data, model parameters, and past disturbance history. This is particularly important in BGC model simulations, because such uncertainties can be spread within the carbon balance over time, leading to the wide range of carbon pool sizes and associated fluxes even by a single model. This is certainly a part of our future work, but nonetheless, this study provides enough evidence of deficiencies in the model structures and formulations of CLM3.5 and the three BGC models, and suggests that such rigorous model evaluations are prerequisite for the interpretation of future climate simulations with full carbon cycle. This study also points to the necessity of data available for assessing key areas of land and BGC model mechanisms, including temporally continuous and finely partitioned storage and respiration measurements, and complementary field studies addressing the diversity of plant functional responses to drought stress in terms of root distributions, vegetation phenology, and stomatal behavior. The closer cooperation between the observational and modeling communities will be indispensable for the developments of the next generation of BGC models.

Appendix A: Photosynthesis in CLM3.5

[53] Photosynthesis is computed in the Community Land Model version 3.5 (CLM3.5) to obtain the stomatal resistance following the relationship [*Collatz et al.*, 1991; *Oleson et al.*, 2004]

$$\frac{1}{r_s} = m\frac{A}{c_s}\frac{e_s}{e_i}P_{atm} + b \tag{A1}$$

where r_s is the stomatal resistance (s m^2 μmolCO$_2^{-1}$), m is a constant depending on Plant Functional Type (PFT), A is photosynthetic activity (μmolCO$_2$ m^{-2} s^{-1}), c_s is the CO$_2$ concentration at the leaf surface (Pa), e_s is the vapor pressure at the leaf surface (Pa), e_i is the saturation vapor pressure inside the leaf that is computed from vegetation temperature, P_{atm} is the atmospheric pressure (Pa), and b is the minimum stomatal resistance (μmolCO$_2$ m^{-2} s^{-1}). A is computed following *Farquhar et al.* [1980] and *Collatz et al.* [1991] as the minimum rate among three processes (here, we limit our description to C3 plants): (1) limitation by light on regeneration of ribulose biphosphate (RuBP), (2) limitation by the amount of the activated RuBP carboxylase, and (3) limitation due to the maximum exporting rate of the photosynthesis products. In the latter two processes, A is dependent on V_{max}, the maximum rate of carboxylation per unit leaf area (μmolCO$_2$ m^{-2} s^{-1}):

$$V_{\max} = N_a F_{LNR}\frac{1}{F_{NR}}a_{25}\left(a_{Q10}\right)^{\frac{T_v-25}{10}}f(T_v)\beta_t f(N) \tag{A2}$$

where N_a is the area-based leaf nitrogen concentration (gN m^{-2} one-sided leaf area, PFT-dependent), F_{LNR} is the fraction of leaf nitrogen in Rubisco (gN$_{Rubisco}$ gN$_{leaf}^{-1}$, PFT-dependent), F_{NR} is the mass ratio of nitrogen in the Rubisco molecule to total molecular mass of Rubisco (gN$_{Rubisco}$ g$_{Rubicso}^{-1}$, constant for all the PFTs), a_{25} is Rubisco activity at 25°C (μmolCO$_2$ gRubisco^{-1} s^{-1}), a_{Q10} is the Q-10 parameter for Rubisco activity, f(T_v) is a function representing inhibition of photosynthesis at high temperature, T_v is the temperature of leaf (K), β_t is a water stress function, and f_N is the nitrogen limitation factor. For the models other than CN, f(N) for each PFT is given in a look-up table derived from a reference simulation of CLM-CN done at National Center for Atmospheric Research. For example, it is set as 0.87 for tropical broadleaf evergreen PFT in CLM3.5 and CASA', and 0.69 in DGVM [*Oleson et al.*, 2008; S. Levis, personal communication, 2010]. f(N) is not applied in CN simulations, instead the nitrogen limitation is included within the carbon allocation algorithm so that plants under insufficient nitrogen to support full growth are forced to allocate smaller carbon in accordance with stoichiometry of carbon and nitrogen in plant tissue. The water stress function β_t is based on the plant wilting factor, w, and the mass fraction of root, r, in each *i*th soil layer;

$$\beta_t = \sum_{i=1}^{10} w_i r_i. \tag{A3}$$

The wilting factor w_i is given as

$$w_i = \begin{cases} \left(\frac{\theta_{sat,i}-\theta_{ice,i}}{\theta_{sat,i}}\right)\left(\frac{\psi_i-\psi_{close}}{\psi_{open}-\psi_{close}}\right) \le 1 & \theta_{liq,i} > 0 \\ 0 & \theta_{liq,i} = 0 \end{cases} \tag{A4}$$

where $\theta_{sat,i}$ is saturated volumetric water content, $\theta_{liq,i}$ is volumetric water content, $\theta_{ice,i}$ is volumetric ice content (m^3 m^{-3}), ψ_i is soil matric potential (mm), and ψ_{open} and

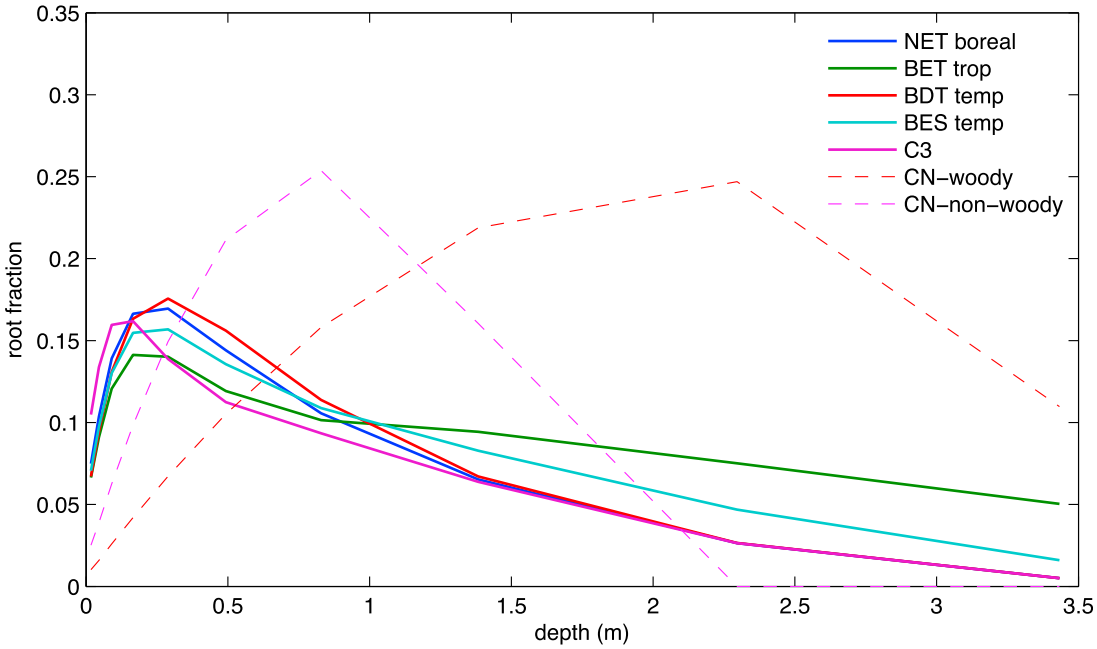

Figure A1. Examples of the vertical distribution of root mass fraction in CLM3.5. The solid lines are the profiles used in the base model CLM3.5 and when it is coupled to CASA' or DGVM. The dashed lines are those used for CLM3.5-CN. NET boreal, needleleaf evergreen boreal tree; BET trop, broadleaf evergreen tropical tree; BDT temp, broadleaf deciduous temperate tree; BES temp, broadleaf evergreen temperate shrub; C3, C3 grass; CN-woody, all the woody PFTs in CN simulation; CN-non-woody, all the nonwoody PFTs in CN simulation.

ψ_{close} are PFT-dependent potentials at which stomata are fully open and closed, respectively. CLM3.5 uses the root fraction distribution from *Zeng* [2001];

$$r_i = \begin{cases} 0.5\left[\begin{array}{l}\exp\left(-r_a z_{h,i-1}\right)+\exp\left(-r_b z_{h,i-1}\right)\\ -\exp\left(-r_a z_{h,i}\right)-\exp\left(-r_b z_{h,i}\right)\end{array}\right] & for\ 1 \le i < 10 \\ 0.5\left[\exp\left(-r_a z_{h,i-1}\right)+\exp\left(-r_b z_{h,i-1}\right)\right] & for\ i = 10 \end{cases} \quad \text{(A5)}$$

where r_a and r_b are PFT-dependant coefficients. CASA' and DGVM also use this form while CN adopts the following distribution

$$r_f(i) = dz(i)\cdot 0.5\left[\left(\frac{2}{z_b}-\frac{2}{z_b^2}z(i-1)\right)+\left(\frac{2}{z_b}-\frac{2}{z_b^2}z(i)\right)\right] \quad \text{(A6)}$$

where z_b is the depth of the bottom interface of the last layer that has nonzero root fraction (3.4 m for woody PFTs, and 1.4 m for nonwoody PFTs), and z(i) is the bottom interface depth of the layer i, and dz(i) is the layer thickness. Equation (A6) gives more root fraction in the deeper soil layer than equation (A5) (Figure A1).

Appendix B: Respiration in CLM3.5 Biogeochemical Submodels

B1. CASA'

[54] The autotrophic respiration (Ra) is assumed to be a constant (0.5) fraction of GPP in CASA'. The heterotrophic respiration (Rh) for each litter and soil organic matter pool is parameterized as a function of carbon (kg C) and sensitivity functions of temperature and soil moisture:

$$R_{h,i} = C_i k_i f_{hT}(T) f_{hw}(\theta) \quad \text{(B1)}$$

where $R_{h,i}$ is the Rh from ith carbon pool, C_i is the amount of carbon, k_i is the maximum decay rate, $f_{hT}(T)$ and $f_{hw}(\theta)$ is the temperature and soil moisture functions to modify the decomposition rate. $f_{hT}(T)$ is an exponential (Q_{10}) function with the base reaction rate ($k_{T,base}$) of 2.0 at 30°C

$$f_{hT} = k_{T,base}^{(T-30)/10} \quad \text{(B2)}$$

where weight-averaged soil temperature from the layers in the top 30cm is used for T. $f_{hw}(\theta)$ is a linear function of the soil wetness.

$$f_{hw} = 0.25 + 0.75s \quad \text{(B3)}$$

s is the soil wetness of the top 30 cm (i.e., the top five model soil layers) defined as

$$s = \sum_{j=1}^{5} \frac{\left[\theta_j - \theta_{w,j}\right]}{\left[\theta_{FC,j} - \theta_{w,j}\right]} w_{soil,j} \quad \text{(B4)}$$

where $w_{soii,j}$ is the fraction of the thickness of each layer to the total soil layer depth.

B2. CN

[55] The maintenance respiration depends on nitrogen content of each tissue and temperature (P. E. Thornton et al., manuscript in preparation, 2010)

$$R_{m,i} = r_{resp} N_i f_{mT}(T) \quad \text{(B5)}$$

where r_{resp} is the base respiration rate per unit nitrogen content (2.525×10^{-6} gC gN^{-1} s^{-1}), N_i is the nitrogen content of each living tissue (leaf, stem, coarse and fine roots), and $f_{mT}(T)$ is a Q_{10} function with the base reaction rate ($k_{T,base}$) of 2.0 at 20°C.

$$f_{mT}(T) = \left(2.525e^{-6}\right)k_{T,base}^{(T-20)/10} \tag{B6}$$

where $2.525e^{-6}$ (gC gN^{-1} s^{-1}) is the respiration base rate per unit nitrogen content. Air temperature at 2m height is used for leaves and stems, and soil temperature is used for fine root. Growth respiration is assumed to be 30% of the total new growth carbon on a given timestep.

[56] Heterotrophic respiration is parameterized as a function of carbon, temperature, soil water content, and available nitrogen in the form of

$$R_{h,i} = C_i k_i f_{hT}(T) f_{hw}(\psi) f_{hN} \tag{B7}$$

The relationship with temperature, f_{hT}, follows the form suggested by *Lloyd and Taylor* [1994] and weight-averaged by the thickness of each layer over the top 30 cm of the soil

$$f_{hT} = \sum_{j=1}^{5}\left\{\exp\left[308.56\left(\frac{1}{71.02} - \frac{1}{T_{soil,j}}\right)\right]w_{soil,j}\right\} \tag{B8}$$

The term within the summation is set to zero when the temperature is below −10°C.

[57] The soil water effect on the decomposition, f_{hw}, is computed from soil water matric potential

$$f_{hw} = \sum_{j=1}^{5}\frac{\log\left(\Psi_{\min}/\Psi_j\right)}{\log\left(\Psi_{\min}/\Psi_{sat,j}\right)}w_{soil,j} \tag{B9}$$

where Ψ_{min} is the minimum soil water potential for decomposition (−10 MPa) and $\Psi_{sat,j}$ is the saturated soil water potential. The nitrogen limitation, f_{hN} is computed from the competitions between the plant and microbial demand for the soil mineral nitrogen.

B3. DGVM

[58] In DGVM, the maintenance respiration of the three living plant tissues, leaf, root, and stem, depends on the amount of carbon and temperature [*Levis et al.*, 2004]

$$R_{m,i} = r_{resp}\frac{C_i}{cn_i}f_{mT}(T) \tag{B10}$$

where r_{resp} is PFT-specific respiration rate (gC gN^{-1} s^{-1}), C is the amount of carbon in g for a given carbon pool, cn is the tissue-specific C:N ratio, and $f_{mT}(T)$ is the sensitivity function suggested by *Lloyd and Taylor* [1994]

$$f_{mT} = \exp\left[308.56\left(\frac{1}{56.02} - \frac{1}{T + 46.02}\right)\right] \tag{B11}$$

where T is the vegetation temperature given in °C for leaf and sapwood, and mean temperature of the top 25 cm soil for root.

[59] For leaf and root maintenance respiration, (B11) is further multiplied by a phenology factor, which represents a fraction of leaves displayed on a pft on a given day, relative to the maximum leaf area index for the year. The growth respiration is assumed to be 25% of GPP minus the sum of maintenance respiration.

[60] Heterotrophic respiration for the two litter and two soil organic pools is similar to that of CASA' (equations (B1) and (B3)), but the Q_{10} temperature response function is replaced with the *Lloyd and Taylor* [1994] relationship (B11).

[61] **Acknowledgments.** We acknowledge LBA, LBA-DMIP, D. C. Nepstad, and TEE project for providing the atmospheric forcing and validation data. The global meteorological data by *Qian et al.* [2006] was provided from NCAR Computational and Information System Laboratory (CISL). We thank Sam Levis and Peter Thornton for providing technical helps regarding the model simulations and formulations. The editor, Dennis Baldocchi, the associate editor, Martin Sykes, and the anonymous reviewer are also thanked for their constructive and helpful comments and suggestions. This work was supported by the National Science Foundation grants ATM-064762 and AGS-0944101.

References

Atkin, O. K., D. Bruhn, V. M. Hurry, and M. G. Tjoelker (2005), The hot and the cold: Unraveling the variable response of plant respiration to temperature, *Funct. Plant Biol.*, *32*, 87–105, doi:10.1071/FP03176.

Baker, I. T., L. Prihodko, A. S. Denning, M. Goulden, S. Miller, and H. R. da Rocha (2008), Seasonal drought stress in the Amazon: Reconciling models and observations, *J. Geophys. Res.*, *113*, G00B01, doi:10.1029/2007JG000644.

Baldocchi, D. D. (2003), Assessing the eddy covariance technique for evaluating carbon dioxide exchange rates of ecosystems: Past, present and future, *Global Change Biol.*, *9*, 479–492, doi:10.1046/j.1365-2486.2003.00629.x.

Belk, E. L., D. Markewitz, T. C. Rasmussen, E. J. M. Carvalho, D. C. Nepstad, and E. A. Davidson (2007), Modeling the effects of throughfall reduction on soil water content in a Brazilian Oxisol under a moist tropical forest, *Water Resour. Res.*, *43*, W08432, doi:10.1029/2006WR005493.

Betts, A. K., and M. A. F. Silva Dias (2010), Progress in understanding land-surface atmospheric coupling from LBA research, *J. Adv. Model. Earth Syst.*, *2*, 6, doi:10.3894/JAMES.2010.2.6.

Betts, R. A., P. M. Cox, M. Collins, P. P. Harris, C. Huntingford, and C. D. Jones (2004), The role of ecosystem-atmosphere interactions in simulated Amazonian precipitation decrease and forest dieback under global climate warming, *Theor. Appl. Climatol.*, *78*, 157–175, doi:10.1007/s00704-004-0050-y.

Bonan, G. B., and S. Levis (2006), Evaluating aspects of the Community Land and Atmospheric Models (CLM3 and CAM3) using a Dynamic Global Vegetation Model, *J. Clim.*, *19*, 2290–2301, doi:10.1175/JCLI3741.1.

Bonan, G. B., S. Levis, S. Sitch, M. Vertenstein, and K. W. Oleson (2003), A dynamic global vegetation model for use with climate models: Concepts and description of simulated vegetation dynamics, *Global Change Biol.*, *9*, 1543–1566, doi:10.1046/j.1365-2486.2003.00681.x.

Brando, P. M., D. C. Nepstad, E. A. Davidson, S. E. Trumbore, D. Ray, and P. Camargo (2008), Drought effects on litterfall, wood production and belowground carbon cycling in an Amazon forest: Results of a throughfall reduction experiment, *Philos. Trans. R. Soc. B*, *363*, 1839–1848, doi:10.1098/rstb.2007.0031.

Brando, P. M., S. J. Goetz, A. Baccini, D. C. Nepstad, P. S. A. Beck, and M. C. Christman (2010), Seasonal and interannual variability of climate and vegetation indices across the Amazon, Proc, *Proc. Natl. Acad. Sci. U. S. A.*, *107*(33), 14,685–14,960, doi:10.1073/pnas.0908741107.

Bruno, R. D., H. R. da Rocha, H. C. de Freitas, M. L. Goulden, and S. D. Miller (2006), Soil moisture dynamics in an eastern Amazonian tropical forest, *Hydrol. Process.*, *20*, 2477–2489, doi:10.1002/hyp.6211.

Carswell, F. E., P. Meir, E. V. Wandelli, C. M. Bonates, B. Kruijt, E. M. Barbosa, A. D. Nobre, J. Grace, and P. G. Jarvis (2000), Photosynthetic capacity in a central Amazonian rain forest, *Tree Physiol.*, *20*, 179–186.

Chambers, J. Q., J. dos Santos, R. J. Ribeiro, and N. Higuchi (2001a), Tree damage, allometric relationships, and above-ground net primary production in central Amazon forest, *For. Ecol. Manage.*, *152*, 73–84, doi:10.1016/S0378-1127(00)00591-0.

Chambers, J. Q., J. P. Schimel, and A. D. Nobre (2001b), Respiration from coarse wood litter in central Amazon forests, *Biogeochemistry*, *52*, 115–131, doi:10.1023/A:1006473530673.

Chambers, J. Q., E. S. Tribuzy, L. C. Toledo, B. F. Crispim, N. Higuchi, J. dos Santos, A. C. Araújo, B. Kruijt, A. D. Nobre, and S. E. Trumbore (2004), Respiration from a tropical forest ecosystem: Partitioning of

sources and low carbon use efficiency, *Ecol. Appl.*, *14*(4), suppl., S72–S88, doi:10.1890/01-6012.

Clapp, R. B., and G. M. Hornberger (1978), Empirical equations for some soil hydraulic properties, *Water Resour. Res.*, *14*(4), 601–604, doi:10.1029/WR014i004p00601.

Collatz, G. J., J. T. Ball, C. Grivet, and J. A. Berry (1991), Physiological and environmental regulation of stomatal conductance, photosynthesis, and transpiration: A model that includes a laminar boundary layer, *Agric. For. Meteorol.*, *54*, 107–136, doi:10.1016/0168-1923(91)90002-8.

Cosby, B. J., G. M. Hornberger, R. B. Clapp, and T. R. Ginn (1984), A statistical exploration of the relationships of soil moisture characteristics to the physical properties of soils, *Water Resour. Res.*, *20*(6), 682–690, doi:10.1029/WR020i006p00682.

Costa, M. H., C. H. C. Oliveira, R. G. Andrade, T. R. Bustamante, F. A. Silva, and M. T. Coe (2002), A macroscale hydrological data set of river flow routing parameters for the Amazon Basin, *J. Geophys. Res.*, *107*(D20), 8039, doi:10.1029/2000JD000309.

Cox, P. M. (2001), *Description of the TRIFFID Dynamic Vegetation Model*, *Tech. Note 24*, Hadley Cent., Met Off., Exeter, U. K.

Cox, P. M., R. A. Betts, M. Collins, P. P. Harris, C. Huntingford, and C. D. Jones (2004), Amazonian forest dieback under climate-carbon cycle projections for the 21st century, *Theor. Appl. Climatol.*, *78*, 137–156, doi:10.1007/s00704-004-0049-4.

da Costa, A. C. L., et al. (2010), Effect of 7 yr of experimental drought on vegetation dynamics and biomass storage of an eastern Amazonian rainforest, *New Phytol.*, *187*, 579–591, doi:10.1111/j.1469-8137.2010.03309.x.

Dai, Y., R. E. Dickinson, and Y.-P. Wang (2004), A two-big-leaf model for canopy temperature, photosynthesis, and stomatal conductance, *J. Clim.*, *17*(12), 2281–2299, doi:10.1175/1520-0442(2004)017<2281:ATMFCT>2.0.CO;2.

da Rocha, H. R., et al. (2009), Patterns of water and heat flux across a biome gradient from tropical forest to savanna in Brazil, *J. Geophys. Res.*, *114*, G00B12, doi:10.1029/2007JG000640.

Davidson, E. A., I. A. Janssens, and Y. Luo (2006), On the variability of respiration in terrestrial ecosystems: Moving beyond Q_{10}, *Global Change Biol.*, *12*, 154–164, doi:10.1111/j.1365-2486.2005.01065.x.

Decker, M., and X. Zeng (2009), Impact of modified Richards equation on global soil moisture simulation in the Community Land Model (CLM3.5), *J. Adv. Model. Earth Syst.*, *1*, 5, doi:10.3894/JAMES.2009.1.5.

Delucia, E. H., J. E. Drake, R. B. Thomas, and M. G. Meler (2007), Forest carbon use efficiency: Is respiration a constant fraction of gross primary production?, *Global Change Biol.*, *13*, 1157–1167, doi:10.1111/j.1365-2486.2007.01365.x.

Desai, A. R., P. R. Moorcroft, P. V. Bolstad, and K. J. Davis (2007), Regional carbon fluxes from an observationally constrained dynamic ecosystem model: Impacts of disturbance, CO_2 fertilization, and heterogenous land cover, *J. Geophys. Res.*, *112*, G01017, doi:10.1029/2006JG000264.

Dickinson, R. E., M. Shaikh, R. Bryant, and L. Graumlich (1998), Interactive canopies for a climate model, *J. Clim.*, *11*, 2823–2836, doi:10.1175/1520-0442(1998)011<2823:ICFACM>2.0.CO;2.

Dickinson, R. E., K. W. Oleson, G. Bonan, F. Hoffman, P. Thornton, M. Vertenstein, Z.-L. Yang, and X. Zeng (2006), The Community Land Model and its climate statistics as a component of the Community Climate System Model, *J. Clim.*, *19*, 2302–2324, doi:10.1175/JCLI3742.1.

Domingues, T. F., J. A. Berry, L. A. Martinelli, J. P. H. B. Ometto, and J. R. Ehleringer (2005), Parameterization of canopy structure and leaf-level gas exchange for an eastern Amazonian tropical rain forest (Tapajós National Forest, Pará, Brazil), *Earth Interact.*, *9*(17), 1–23, doi:10.1175/EI149.1.

Doney, S. C., K. Lindsay, I. Fung, and J. John (2006), Natural variability in a stable, 1000-Yr global coupled climate-carbon cycle simulation, *J. Clim.*, *19*, 3033–3054, doi:10.1175/JCLI3783.1.

Doughty, C. E., and M. L. Goulden (2008a), Seasonal patterns of tropical forest leaf area index and CO_2 exchange, *J. Geophys. Res.*, *113*, G00B06, doi:10.1029/2007JG000590.

Doughty, C. E., and M. L. Goulden (2008b), Are tropical forests near a high temperature threshold?, *J. Geophys. Res.*, *113*, G00B07, doi:10.1029/2007JG000632.

Doughty, C. E., M. L. Goulden, S. D. Miller, and H. R. da Rocha (2006), Circadian rhythms constrain leaf and canopy gas exchange in an Amazonian forest, *Geophys. Res. Lett.*, *33*, L15404, doi:10.1029/2006GL026750.

Eltahir, E. A. B., and R. L. Bras (1994), Precipitation recycling in the Amazon basin, *Q. J. R. Meteorol. Soc.*, *120*, 861–880, doi:10.1002/qj.49712051806.

Farquhar, G. D., S. von Caemmerer, and J. A. Berry (1980), A biochemical model of photosynthetic CO_2 assimilation in leaves of C_3 species, *Planta*, *149*, 78–90, doi:10.1007/BF00386231.

Fisher, R. A., M. Williams, R. L. Do Vale, A. L. da Costa, and P. Meir (2006), Evidence from Amazonian forests is consistent with isohydric control of leaf water potential, *Plant Cell Environ.*, *29*, 151–165, doi:10.1111/j.1365-3040.2005.01407.x.

Fisher, R. A., M. Williams, A. L. da Costa, Y. Malhi, R. F. da Costa, S. Almeida, and P. Meir (2007), The response of an eastern Amazonian rain forest to drought stress: Results and modeling analyses from a throughfall exclusion experiment, *Global Change Biol.*, *13*, 2361–2378, doi:10.1111/j.1365-2486.2007.01417.x.

Fisher, R. A., N. McDowell, D. Purves, P. Moorcroft, S. Stich, P. Cox, C. Huntingford, P. Meir, and F. I. Woodward (2010), Assessing uncertainties in a second-generation dynamic vegetation model caused by ecological scale limitations, *New Phytol.*, *187*, 666–681, doi:10.1111/j.1469-8137.2010.03340.x.

Foley, J. A., C. Prentice, N. Ramankutty, S. Levis, D. Pollard, S. Sitch, and A. Haxeltine (1996), An integrated biosphere model of land surface processes, terrestrial carbon balance, and vegetation dynamics, *Global Biogeochem. Cycles*, *10*(4), 603–628, doi:10.1029/96GB02692.

Friedlingstein, P., G. Joel, C. B. Field, and I. Y. Fung (1999), Toward an allocation scheme for global terrestrial carbon models, *Global Change Biol.*, *5*, 755–770, doi:10.1046/j.1365-2486.1999.00269.x.

Friedlingstein, P., et al. (2006), Climate-carbon cycle feedback analysis: Results from the C^4 MIP model intercomparison, *J. Clim.*, *19*, 3337–3353, doi:10.1175/JCLI3800.1.

Fung, I. Y., S. C. Doney, K. Lindsay, and J. John (2004), Evolution of carbon sinks in a changing climate, *Proc. Natl. Acad. Sci. U. S. A.*, *102*(32), 11,201–11,206, doi:10.1073/pnas.0504949102.

Fyllas, N. M., et al. (2009), Basin-wide variations in foliar properties of Amazonian forest: Phylogeny, soils and climate, *Biogeosciences*, *6*, 2677–2708, doi:10.5194/bg-6-2677-2009.

Galbraith, D., P. E. Levy, S. Sitch, C. Huntingford, P. Cox, M. Williams, and P. Meir (2010), Multiple mechanisms of Amazonian forest biomass losses in three dynamic global vegetation models under climate change, *New Phytol.*, *187*, 647–665, doi:10.1111/j.1469-8137.2010.03350.x.

Houghton, R. A., K. T. Lawrence, J. L. Hackler, and S. Brown (2001), The spatial distribution of forest biomass in the Brazilian Amazon: A comparison of estimates, *Global Change Biol.*, *7*, 731–746, doi:10.1046/j.1365-2486.2001.00426.x.

Huan, M., G. P. Asner, M. Keller, and J. A. Berry (2008), An ecosystem model for tropical forest disturbance and selective logging, *J. Geophys. Res.*, *113*, G01002, doi:10.1029/2007JG000438.

Huete, A. R., K. Didan, Y. E. Shimabukuro, P. Ratana, S. R. Saleska, L. R. Hutrya, W. Yang, R. R. Nemani, and R. Myneni (2006), Amazon rainforests green-up with sunlight in dry season, *Geophys. Res. Lett.*, *33*, L06405, doi:10.1029/2005GL025583.

Huntingford, C., et al. (2008), Towards quantifying uncertainty in predictions of Amazon 'dieback,' *Philos. Trans. R. Soc. B*, *363*, 1857–1864, doi:10.1098/rstb.2007.0028.

Hutyra, L. R., J. W. Munger, C. A. Nobre, S. R. Saleska, S. A. Vieira, and S. C. Wofsy (2005), Climatic variability and vegetation vulnerability in Amazônia, *Geophys. Res. Lett.*, *32*, L24712, doi:10.1029/2005GL024981.

Hutyra, L. R., J. W. Munger, S. R. Saleska, E. Gottlieb, B. C. Daube, A. L. Dunn, D. F. Amaral, P. B. de Camargo, and S. C. Wofsy (2007), Seasonal controls on the exchange of carbon and water in an Amazonian rain forest, *J. Geophys. Res.*, *112*, G03008, doi:10.1029/2006JG000365.

Keller, M., et al. (2004), Ecological research in the Large-Scale Biosphere-Atmosphere experiment in Amazonia: Early results, *Ecol. Appl.*, *14*(4), suppl., S3–S16, doi:10.1890/03-6003.

Khomik, M., M. A. Arain, K.-L. Liaw, and J. H. McCaughty (2009), Debut of a flexible model for simulating soil respiration-soil temperature relationship: Gamma model, *J. Geophys. Res.*, *114*, G03004, doi:10.1029/2008JG000851.

Kucharik, C. J., J. A. Foley, C. Delire, V. A. Fisher, M. T. Coe, J. D. Lenters, C. Y. Molling, and N. Ramankutty (2000), Testing the performance of a Dynamic Global Ecosystem Model: Water balance, carbon balance, and vegetation structure, *Global Biogeochem. Cycles*, *14*(3), 795–825, doi:10.1029/1999GB001138.

Kucharik, C. J., C. C. Barford, M. El Maayar, S. C. Wofsy, R. K. Monson, and D. D. Baldocchi (2006), A multiyear evaluation of a Dynamic Global Vegetation Model at three Ameriflux forest sites: Vegetation structure, phenology, soil temperature, and CO_2 and H_2O vapor exchange, *Ecol. Modell.*, *196*, 1–31, doi:10.1016/j.ecolmodel.2005.11.031.

Lawrence, D. M., P. E. Thornton, K. W. Oleson, and G. Bonan (2007), The partitioning of evapotranspiration into transpiration, soil evaporation, and canopy evaporation in a GCM: Impacts on land-atmosphere interaction, *J. Hydrometeorol.*, *8*, 862–880, doi:10.1175/JHM596.1.

Lee, J.-E., R. S. Oliveira, T. E. Dawson, and I. Fung (2005), Root functioning modifies seasonal climate, *Proc. Natl. Acad. Sci. U. S. A.*, *102*(49), 17,576–17,581, doi:10.1073/pnas.0508785102.

Levis, S., G. B. Bonan, M. Vertenstein, and K. W. Oleson (2004), The community Land Model's Dynamic Global Vegetation Model (CLM-DGVM): Technical description and user's guide, *NCAR Tech. Note NCAR/TN-459+IA*, 50 pp., Natl. Cent. for Atmos. Res., Boulder, Colo.

Lloyd, J., and G. D. Farquhar (2008), Effects of rising temperatures and [CO_2] on the physiology of tropical forest trees, *Philos. Trans. R. Soc. B*, *363*, 1811–1817, doi:10.1098/rstb.2007.0032.

Lloyd, J., and J. A. Taylor (1994), On the temperature dependence of soil respiration, *Funct. Ecol.*, *8*, 315–323, doi:10.2307/2389824.

Malhi, Y. L. E., et al. (2006), The regional variation of aboveground live biomass in old-growth Amazonian forests, *Global Change Biol.*, *12*, 1107–1138, doi:10.1111/j.1365-2486.2006.01120.x.

Malhi, Y., J. T. Roberts, R. A. Betts, T. J. Killeen, W. Li, and C. A. Nobre (2008), Climate change, deforestation, and the fate of the Amazon, *Science*, *319*, 169–172, doi:10.1126/science.1146961.

Malhi, Y., L. E. O. C. Aragão, D. Galbraith, C. Huntingford, R. Fisher, P. Zelazowski, S. Sitch, C. McSweeney, and P. Meir (2009a), Exploring the likelihood and mechanism of a climate-change-induced dieback of the Amazon rainforest, *Proc. Natl. Acad. Sci. U. S. A.*, *106*(49), 20,610–20,615, doi:10.1073/pnas.0804619106.

Malhi, Y., et al. (2009b), Comprehensive assessment of carbon productivity, allocation and storage in three Amazonian forests, *Global Change Biol.*, *15*, 1255–1274, doi:10.1111/j.1365-2486.2008.01780.x.

Markewitz, D., E. Davidson, P. Moutinho, and D. Nepstad (2004), Nutrient loss and redistribution after forest clearing on a highly weathered soil in Amazonia, *Ecol. Appl.*, *14*(4), S177–S199, doi:10.1890/01-6016.

McDowell, N., et al. (2008), Mechanisms of plant survival and mortality during drought: Why do some plants survive while others succumb to drought?, *New Phytol.*, *178*, 719–739, doi:10.1111/j.1469-8137.2008.02436.x.

Medvigy, D., S. C. Wofsy, J. W. Munger, D. Y. Hollinger, and P. R. Moorcroft (2009), Mechanistic scaling of ecosystem function and dynamics in space and time: Ecosystem Demography model version 2, *J. Geophys. Res.*, *114*, G01002, doi:10.1029/2008JG000812.

Meehl, G. A., et al. (2007), Global climate projections, in *Climate Change 2007: The Physical Science Basis. Contribution of Working Group I to the Fourth Assessment Report of the Intergovernmental Panel on Climate Change*, edited by S. Solomon et al., Cambridge Univ. Press, New York.

Meir, P., D. B. Metcalfe, A. C. L. Costa, and R. A. Fisher (2008), The fate of assimilated carbon during drought: Impacts on respiration in Amazonian rainforests, *Philos. Trans. R. Soc. B*, *363*, 1849–1855, doi:10.1098/rstb.2007.0021.

Moorcroft, P. R. (2006), How close are we to a predictive science of the biosphere?, *Trends Ecol. Evol.*, *21*(7), 400–407, doi:10.1016/j.tree.2006.04.009.

Moorcroft, P. R., G. C. Hurtt, and S. W. Pacala (2001), A method for scaling vegetation dynamics: The Ecosystem Demography model (ED), *Ecol. Monogr.*, *71*(4), 557–586, doi:10.1890/0012-9615(2001)071[0557:AMFSVD]2.0.CO;2.

NASA (2007), Monthly 0.25° × 0.25° TRMM and other sources rainfall, Distrib. Active Arch. Cent., Earth Sci., Goddard Space Flight Cent., Greenbelt, Md. (Available at http://mirador.gsfc.nasa.gov/cgi-bin/mirador/presentNavigation.pl?tree=project&project=TRMM&dataGroup = Gridded&data set=3B43:%20Monthly%200.25%20x%200.25%20degree%20merged%20TRMM%20and%20 other%20sources%20estimates&version=006)

Nepstad, D. C., and P. R. Mountinho (2008a), LBA-ECO LC-14 Rainfaill Exclusion Experiment, Canopy Density, TNF, Brazil: 1999–2005, data set, LBA Data and Inf. Syst., Natl. Inst. for Space Res. (INPE/CPTEC), Cachoeira Paulista, Sao Paulo, Brazil. (Available at http://lba.cptec.inpe.br/)

Nepstad, D. C., and P. R. Mountinho (2008b), LBA-ECO LC-14 Rainfaill Exclusion Experiment, LAI, Gap Fraction, TNF, Brazil: 2000–2005, data set, LBA Data and Inf. Syst., Natl. Inst. for Space Res. (INPE/CPTEC), Cachoeira Paulista, Sao Paulo, Brazil. (Available at http://lba.cptec.inpe.br/)

Nepstad, D. C., and P. R. Mountinho (2009a), LBA-ECO LC-14 Rainfaill Exclusion Experiment, Specific Leaf Area, TNF, Brazil, data set, LBA Data and Inf. Syst., Natl. Inst. for Space Res. (INPE/CPTEC), Cachoeira Paulista, Sao Paulo, Brazil. (Available at http://lba.cptec.inpe.br/)

Nepstad, D. C., and P. R. Mountinho (2009b), LBA-ECO LC-14 Rainfaill Exclusion Experiment, Volumetric Soil Water, TNF, Brazil, data set, LBA Data and Inf. Syst., Natl. Inst. for Space Res. (INPE/CPTEC), Cachoeira Paulista, Sao Paulo, Brazil. (Available at http://lba.cptec.inpe.br/)

Nepstad, D. C., and P. R. Mountinho (2010), LBA-ECO LC-14 Rainfaill Exclusion Experiment, Fine Litter Production, TNF, Brazil, data set, LBA Data and Inf. Syst., Natl. Inst. for Space Res. (INPE/CPTEC), Cachoeira Paulista, Sao Paulo, Brazil. (Available at http://lba.cptec.inpe.br/)

Nepstad, D. C., et al. (2002), The effects of partial throughfall exclusion on canopy processes, aboveground production, and biogeochemistry of an Amazon forest, *J. Geophys. Res.*, *107*(D20), 8085, doi:10.1029/2001JD000360.

Nepstad, D. C., I. M. Toshver, D. Ray, P. Moutinho, and G. Cardinot (2007), Mortality of large trees and lianas following experimental drought in an Amazon forest, *Ecology*, *88*(9), 2259–2269, doi:10.1890/06-1046.1.

Niu, G.-Y., Z.-L. Yang, R. E. Dickinson, L. E. Gulden, and H. Su (2007), Development of a simple groundwater model for use in climate models and evaluation with Gravity Recovery and Climate Experiment data, *J. Geophys. Res.*, *112*, D07103, doi:10.1029/2006JD007522.

Oleson, K. W., et al. (2004), Technical description of the Community Land Model (CLM), *NCAR Tech. Note NCAR/TN-461+STR*, 173 pp., Natl. Cent. for Atmos. Res., Boulder, Colo.

Oleson, K. W., et al. (2008), Improvements to the Community Land Model and their impact on the hydrological cycle, *J. Geophys. Res.*, *113*, G01021, doi:10.1029/2007JG000563.

Oleson, K. W., et al. (2010), Technical description of version 4.0 of the Community Land Model, *NCAR Tech. Note NCAR/TN-478+STR*, 257 pp., Natl. Cent. for Atmos. Res., Boulder, Colo.

Oliveira, R. S., T. E. Dawson, S. S. O. Burgess, and D. C. Nepstad (2005), Hydraulic redistribution in three Amazonian trees, *Oecologia*, *145*, 354–363, doi:10.1007/s00442-005-0108-2.

Oyama, M. D., and C. F. Nobre (2003), A new climate-vegetation equilibrium state for tropical South America, *Geophys. Res. Lett.*, *30*(32), 2199, doi:10.1029/2003GL018600.

Phillips, O. L., et al. (2009), Drought sensitivity of the Amazon rainforest, *Science*, *323*, 1344–1346, doi:10.1126/science.1164033.

Potter, C. S. (1999), Terrestrial biomass and the effects of deforestation on the global carbon cycle, *BioScience*, *49*(10), 769–778, doi:10.2307/1313568.

Potter, C. S., J. T. Randerson, C. B. Field, P. A. Matson, P. M. Vitousek, H. A. Mooney, and S. A. Klooster (1993), Terrestrial ecosystem production: A process model based on global satellite and surface data, *Global Biogeochem. Cycles*, *7*(4), 811–841, doi:10.1029/93GB02725.

Purves, D., and S. Pacala (2008), Predictive models of forest dynamics, *Science*, *320*, 1452–1453, doi:10.1126/science.1155359.

Pyle, E. H., et al. (2008), Dynamics of carbon, biomass, and structure in two Amazonian forests, *J. Geophys. Res.*, *113*, G00B08, doi:10.1029/2007JG000592.

Qian, T., A. Dai, K. E. Trenberth, and K. W. Oleson (2006), Simulation of global land surface conditions from 1948 to 2004. Part I: Forcing data and evaluations, *J. Hydrometeorol.*, *7*, 953–975, doi:10.1175/JHM540.1.

Quesada, C. A., J. Lloyd, L. O. Anderson, N. M. Fyllas, M. Schwarz, and C. I. Czimczik (2009), Soils of Amazonia with particular reference to the rainfor sites, *Biogeosciences Discuss.*, *6*, 3851–3921, doi:10.5194/bgd-6-3851-2009.

Randerson, J. T., et al. (2009), Systematic assessment of terrestrial biogeochemistry in coupled climate-carbon models, *Global Change Biol.*, doi:10.1111/j.1365-2486.2009.01912.x.

Restrepo-Coupe, N. (2007), BRASILFLUX quality control procedure, report, Univ. of Ariz., Tucson.

Rice, A. H., E. H. Pyle, S. R. Saleska, L. Hutyra, M. Palace, M. Keller, P. B. de Camargo, K. Portilho, D. F. Marques, and S. C. Wofsy (2004), Carbon balance and vegetation dynamics in an old-growth Amazonian forest, *Ecol. Appl.*, *14*(4), suppl., S55–S71, doi:10.1890/02-6006.

Salazar, L. F., C. A. Nobre, and M. D. Oyama (2007), Climate change consequences on the biome distribution in tropical South America, *Geophys. Res. Lett.*, *34*, L09708, doi:10.1029/2007GL029695.

Saleska, S. R., et al. (2003), Carbon in Amazonian forests: Unexpected seasonal fluxes and disturbance-induced losses, *Science*, *302*, 1554–1557, doi:10.1126/science.1091165.

Saleska, S. R., K. Didan, A. R. Huete, and H. R. da Rocha (2007), Amazon forests green-up during 2005 drought, *Science*, *318*, 612, doi:10.1126/science.1146663.

Samanta, A., S. Gauguly, H. Hashimoto, S. Devadiga, E. Vermote, Y. Knyazikhin, R. R. Nemani, and R. B. Myneni (2010), Amazon forests did not green-up during the 2005 drought, *Geophys. Res. Lett.*, *37*, L05401, doi:10.1029/2009GL042154.

Silver, W. L., J. Neff, M. McGroddy, E. Veldkamp, M. Keller, and R. Cosme (2000), Effects of soil texture on belowground carbon and nutrient storage in a lowland Amazonian forest ecosystem, *Ecosystems*, *3*, 193–209, doi:10.1007/s100210000019.

Sitch, S., et al. (2003), Evaluation of ecosystem dynamics, plant geography and terrestrial carbon cycling in the LPJ dynamic global vegetation model, *Global Change Biol.*, *9*, 161–185, doi:10.1046/j.1365-2486.2003.00569.x.

Sitch, S., et al. (2008), Evaluation of the terrestrial carbon cycle, future plant geography and climate-carbon cycle feedbacks using five Dyna-

mice Global Vegetation Models (DGVMs), *Global Change Biol.*, *14*, 2015–2039, doi:10.1111/j.1365-2486.2008.01626.x.

Smith, B., I. C. Prentice, and M. T. Sykes (2001), Representation of vegetation dynamics in the modeling of terrestrial ecosystems: Comparing two contrasting approaches within European climate space, *Glob. Ecol. Biogeogr.*, *10*, 621–637, doi:10.1046/j.1466-822X.2001.00256.x.

Sotta, E. D., E. Veldkamp, L. Schwendenmann, B. R. Guimarães, R. K. Paixão, M. de Lourdes, P. Ruivo, A. C. L. da Costa, and P. Meir (2007), Effects of an induced drought on soil carbon dioxide (CO_2) efflux and soil CO_2 production in an Eastern Amazonian rainforest, Brazil, *Global Change Biol.*, *13*, 2218–2229, doi:10.1111/j.1365-2486.2007.01416.x.

Sperry, J. S., F. R. Adler, G. S. Campbell, and J. P. Comstock (1998), Limitation of plant water use by rhizosphere and xylem conductance: Results from a model, *Plant Cell Environ.*, *21*, 347–359, doi:10.1046/j.1365-3040.1998.00287.x.

Stöckli, R., D. M. Lawrence, G.-Y. Niu, K. W. Oleson, P. E. Thornton, Z.-L. Yang, G. B. Bonan, A. S. Denning, and S. W. Running (2008a), Use of FLUXNET in the Community Land Model development, *J. Geophys. Res.*, *113*, G01025, doi:10.1029/2007JG000562.

Stöckli, R., T. Rutishauser, D. Dragoni, J. O'Keefe, P. E. Thornton, M. Jolly, L. Lu, and A. S. Denning (2008b), Remote sensing data assimilation for a prognostic phenology model, *J. Geophys. Res.*, *113*, G04021, doi:10.1029/2008JG000781.

Taylor, K. E., R. J. Stouffer, and G. A. Meehl (2009), A summary of the CMIP5 experimental design, CMIP5 Experimental Design Document, World Clim. Res. Programme, Geneva. (Available at http://cmip-pcmdi.llnl.gov/cmip5/experiment_design.html?submenuheader=1)

Thonicke, K., S. Venensky, S. Sitch, and W. Cramer (2001), The role of fire disturbance for global vegetation dynamics: Coupling fire into a Dynamic Global Vegetation Model, *Glob. Ecol. Biogeogr.*, *10*, 661–677, doi:10.1046/j.1466-822X.2001.00175.x.

Thornton, P. E., and N. A. Rosenbloom (2005), Ecosystem model spin-up: Estimating steady state conditions in a coupled terrestrial carbon and nitrogen model, *Ecol. Modell.*, *189*, 25–48, doi:10.1016/j.ecolmodel.2005.04.008.

Thornton, P. E., and N. E. Zimmermann (2007), An improved canopy integration scheme for a land surface model with prognostic canopy structure, *J. Clim.*, *20*, 3902–3923, doi:10.1175/JCLI4222.1.

Thornton, P. E., et al. (2002), Modeling and measuring the effects of disturbance history and climate on carbon and water budgets in evergreen needleleaf forests, *Agric. For. Meteorol.*, *113*, 185–222, doi:10.1016/S0168-1923(02)00108-9.

Thornton, P. E., S. C. Doney, K. Lindsay, J. K. Moore, N. Mahowald, J. T. Randerson, I. Fung, J.-F. Lamarque, J. J. Feddema, and Y.-H. Lee (2009), Carbon-nitrogen interactions regulate climate-carbon cycle feedbacks: Results from an atmosphere-ocean general circulation model, *Biogeosciences*, *6*, 2099–2120, doi:10.5194/bg-6-2099-2009.

Watanabe, T., M. Yokozawa, S. Emori, K. Takata, A. Sumida, and T. Hara (2002), Developing a multi-layered integrated numerical model of surface physics—Growing plants interaction (MINoSGI), *Global Change Biol.*, *10*, 963–982, doi:10.1111/j.1529-8817.2003.00768.x.

White, M. A., P. E. Thornton, and S. W. Running (1997), A continental phenology model for monitoring vegetation responses to interannual climatic variability, *Global Biogeochem. Cycles*, *11*(2), 217–234, doi:10.1029/97GB00330.

Wilson, K., et al. (2002), Energy balance closure at FLUXNET sites, *Agric. For. Meteorol.*, *113*, 223–243, doi:10.1016/S0168-1923(02)00109-0.

Wright, I. J., P. B. Reich, O. K. Atkin, C. H. Luck, M. G. Tjoelker, and M. Westoby (2006), Irradiance, temperature and rainfall influence leaf dark respiration in woody plants: Evidence from comparisons across 20 sites, *New Phytol.*, *169*, 309–319, doi:10.1111/j.1469-8137.2005.01590.x.

Zeng, X. (2001), Global vegetation root distribution for land modeling, *J. Hydrometeorol.*, *2*, 525–530, doi:10.1175/1525-7541(2001)002<0525:GVRDFL>2.0.CO;2.

Zeng, X., and M. Decker (2009), Improving the numerical solution of soil moisture-based Richards equation for land models with a deep or shallow water table, *J. Hydrometeorol.*, *10*, 308–319, doi:10.1175/2008JHM1011.1.

Zeng, X. D., X. Zeng, and M. Barlage (2008), Growing temperate shrubs over arid and semiarid regions in the Community Land Model-Dynamic Global Vegetation Model, *Global Biogeochem. Cycles*, *22*, GB3003, doi:10.1029/2007GB003014.

Zhou, T., P. Shi, D. Hui, and Y. Luo (2009), Global pattern of temperature sensitivity of soil heterotrophic respiration (Q_{10}) and its implications for carbon-climate feedback, *J. Geophys. Res.*, *114*, G02016, doi:10.1029/2008JG000850.

P. M. Brando, Instituto de Pesquisa Ambiental da Amazônia, SHIN CA-5, Lote J2, Bloco J2, Brasilia, DF, CEP 71503-505, Brazil.

B. J. Christoffersen, N. Restrepo-Coupe, and S. R. Saleska, Department of Ecology and Evolutionary Biology, University of Arizona, BioSciences W. Bldg., 1041 E. Lowell St., Tucson, AZ 85721, USA.

K. Sakaguchi and X. Zeng, Department of Atmospheric Sciences, University of Arizona, Physics-Atmospheric Sciences Bldg., 1118 E. 4th St., Tucson, AZ 85721, USA. (ksa@email.arizona.edu)